PART IV

Developments of Nanocomposites/Coatings for Special Applications

CHAPTER 17

Polytetrafluoroethylene matrix nanocomposites for tribological applications

David L. Burris, Katherine Santos, Sarah L. Lewis, Xinxing Liu, Scott S. Perry, Thierry A. Blanchet, Linda S. Schadler and W. Gregory Sawyer

Contents

Abstract

Solid lubricants comprise an important class of materials and find use in applications where the use of more traditional lubrication techniques is undesirable or precluded. Polytetrafluoroethylene (PTFE) is a notable solid lubricant material, being known for its reputably low friction coefficient, high thermal range and chemical resistance, but a high wear rate limits its application in moving mechanical systems. The use of microfillers can reduce the wear rates to more acceptable values, but large particle size, high filler concentration, increased abrasion and increased friction coefficient all contribute to limit the performance of the composite. The use of nanofillers has been shown to provide further improvements in wear rates without introducing detrimental effects on its other beneficial properties. This work outlines recent studies of the wear resistance mechanisms in these novel systems. Several key wear resistance mechanisms have been identified: (1) bonding and strength at the filler/matrix interface, (2) dispersion and mechanical effects of load support and crack deflection, (3) morphological effects of nanoparticles on the matrix, (4) fibrillation and toughening, (5) transfer film coverage, (6) transfer film orientation and (7) chemical degradation. It is found that the ca. 1,000X improvement in wear resistance that trace loadings of nanofillers impart to PTFE is due to a synergism of wear resistance mechanisms that is activated by the small filler size.

17.1 Introduction

17.1.1 Motivation and organization

Proper lubrication enables the smooth operation of nearly all moving devices we use on a daily basis, from cabinet drawers to automobiles. Traditional fluid and grease lubricants are ideal for many applications and provide characteristically low friction coefficients and wear rates, but in an increasing number of applications, these lubrication techniques may be impractical or even precluded. The reservoirs, pumps and filters required in fluid lubricated systems add cost, size and weight, and grease re-application may be prohibitive. Fluid and grease lubricants also have inherent environmental limitations. They can be contaminated by dirt and debris and can themselves lead to contamination

of the product or the environment. Furthermore, they outgas in low pressure and vacuum applications and function only over limited temperature ranges.

Solid lubricants are often used in applications where fluid and grease lubricants do not provide the required performance. Solid lubricants provide a number of advantages including low cost, simplicity, structural integrity and environmental insensitivity. Most importantly, however, solid lubricants provide lubrication internally and do not require external lubricants for successful operation. Because the low friction mechanism in solid lubricants often involves failure at weak internal interfaces, self-lubricated systems generally exhibit higher friction and wear than fluid and grease-lubricated systems. Significant research efforts are currently dedicated to reducing friction and wear at self-lubricated interfaces and deducing the mechanisms by which solid lubricants operate.

Typically self-lubricated bearings entail either bulk bushings or slideways of polymers or polymer composites, or thin coatings of lamellar solids such as molybdenum disulfide or graphite. PTFE is a common solid lubricant used for its unique combination of low friction, low chemical reactivity and large operational temperature range. Its applications include nonstick frying pan coatings, low friction seals, oil additives and vascular stents. Despite its promising combination of unique physical properties and widespread use in engineering, the high wear rate of PTFE has greatly limited its use as a solid lubricant. The goal of the work summarized here is to identify mechanisms of wear and wear resistance in PTFE composites to guide the future design of low-wear PTFE-based solid lubricants. The remainder of this chapter is organized as follows:

In the introduction, we examine and discuss the PTFE tribology literature of unfilled, filled and nanofilled PTFE-based tribosystems. In the following section, initial findings of a multi-university collaboration focusing on the fundamental mechanisms in PTFE-based tribosystems are discussed. The chapter concludes by offering a hypothesized model of PTFE wear resistance that is based on a combination of the literature with findings from the current research. Properties and wear resistance mechanisms of PTFE nanocomposites are discussed and the importance of synergies is highlighted; it is suggested that 100X improvements in wear resistance can be achieved with any of several wear resistance mechanisms, but 10,000X improvements are only achieved through synergies unique to nanocomposites.

17.1.2 Polytetrafluoroethylene as a solid lubricant

PTFE is a linear chain polymer of smooth molecular profile consisting of 20,000–200,000 repeating units of tetrafluoroethylene (C_2F_4). The fluorine encasement of the carbon backbone provides high chemical inertness, while its smooth profile provides low friction sliding. PTFE also has a large useful temperature range (4–500 K) and a very low vapor pressure (low outgassing) making it a viable material for solid lubrication in space.

PTFE is viscoelastic in nature and as a result, its tribological properties are strong functions of both sliding speed and temperature. As temperature is reduced or speed increased, the friction coefficient increases [1–6]. In low speed (<10 mm/s) applications PTFE has a low friction coefficient (between $\mu = 0.03$ and $\mu = 0.1$) and moderate wear resistance (10^{-5} mm^3/N m). Makinson and Tabor [3] found that as the sliding speed increased to above 10 mm/s at room temperature, a transition from mild to severe wear (10^{-5}–10^{-3} mm^3/N m) accompanied increased friction. They combined the early structural work of Bunn, Cobold and Palmer [7], and Speerschnieder and Li [8] with their own tribological results and electron diffraction work to relate the tribological behavior of PTFE to deformation of its crystalline structure. They hypothesized that at conditions of both low speed (<10 mm/s) and high temperature ($>30\,^\circ$C), shearing occurs in the rate sensitive amorphous regions giving rise to a lamellar-type response of crystals or molecules. As speed is increased or temperature decreased from an original condition of low friction and moderate wear, the stress required to shear amorphous regions exceeds the stress required to cause failure at boundaries between crystalline regions in the sintered material. They concluded that this leads to larger debris and increased wear rates. Tanaka proposed a similar model with failure occurring at boundaries of the characteristic "banded" structure of PTFE [6]. Blanchet

and Kennedy [1] studied this severe wear transition at several temperatures and found an increase in the transition speed to accompany increased temperature. When the wear rate, k, was plotted versus the friction coefficient, μ, the transition to severe wear occurred at $\mu = 0.1$ in each case. These results are consistent with the proposed transition mechanism of Makinson and Tabor [3] and suggest that the severe wear transition is a response to the stress state and thus the friction coefficient, while the friction coefficient is a function of both speed and temperature. Several samples were microtomed perpendicular to the wear surface in the direction of sliding after mild and severe wear had taken place. Cracks were found to propagate in the direction of sliding beneath a layer of worked material at subsurface depths consistent with observed debris thicknesses for severe wear samples. No such cracks were found in mild wear samples. They conjectured that defects in the sintered material act as initiated cracks. When speeds are low, the kinetic friction coefficient at the tribological interface is low, and the static friction coefficient between internal crack faces is sufficient to fully support the surface tractions. However, when the kinetic coefficient of friction at the tribological interface increases with increased sliding speed and exceeds the static coefficient of friction ($\mu \sim 0.1$) at internal PTFE/PTFE interfaces, the crack tips must support shear. This leads to a progressive delamination wear process similar to that described in Suh's delamination theory of wear [9]. The severe wear of PTFE at speeds greater than the temperature-dependent transition speed has precluded its use in many applications, and motivates the use of fillers to abate the onset of severe wear.

17.1.3 PTFE-based tribological composites

For decades, fillers have been successfully used to reduce the wear of PTFE. In Fig. 17.1, wear rate is plotted versus filler wt% for testing of some representative PTFE composites found in the literature [10–15]. Despite being tested with varying configurations, testers, methods, pressures, speeds and fillers, there is a systematic trend of decreased wear rate with increased filler fraction up to 50 wt%.

The wear reducing mechanism of fillers in PTFE-based composites remains a topic of debate. Lancaster [16] proposed that the hard wear-resistant fillers, especially those with a high aspect ratio,

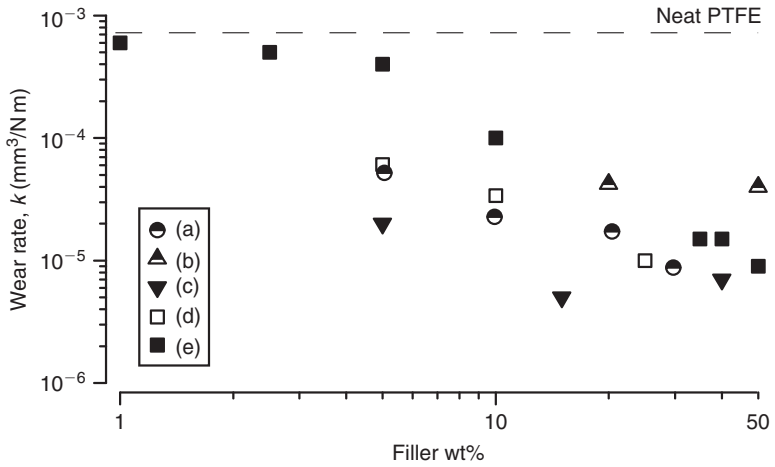

Fig. 17.1. Wear rate versus filler fraction for some of the PTFE-based microcomposite systems found in the tribology literature: (a) Li et al. (2000) – graphite, (b) Bahadur and Gong (1992) – graphite, (c) Lu et al. (1995) – PEEK, (d) Burroughs et al. (1999) – B_2O_3, (e) Menzel and Blanchet (2002) – irradiated FEP. Neat PTFE has a high wear rate ($k \sim 10^{-3}$ mm^3/N m) at speeds above 10 mm/s, while composites approach a moderate wear rate ($k \sim 10^{-5}$ mm^3/N m) as filler fraction increases above 10 wt%.

preferentially support the load, reducing the wear of PTFE in the composite. Sung and Suh [17] found that vertically oriented fibers were most effective in reducing wear, but suggested that the critical role of the filler was to arrest crack propagation, rather than to support the load. Tanaka et al. [6, 18] suggested that the filler prevented the initial transfer of the PTFE to the counterface, and thus prevented transfer wear. Briscoe [19] noted the formation of a thin, well-adhered transfer film for a high-density polyethylene system and hypothesized that fillers provide augmented transfer film adhesion, and thus reduced transfer wear by slowing transfer film removal and the requisite replenishment. Using X-Ray photoelectron spectroscopy (XPS), Gong et al. [20, 21] found that the wear rate of PTFE was independent of chemical bonding with the counterface, and concluded that cohesive failure within the PTFE must govern its wear rate. Blanchet et al. had similar findings with XPS analysis of PTFE and PTFE composites in dry sliding, and concluded that the wear reducing role of the filler is to slow primary removal of material from the bulk by arresting crack propagation rather than slowing secondary removal of material from the counterface via increased transfer film adhesion [22]. Bahadur and Tabor [23] and Blanchet and Kennedy [1] saw direct relationships between wear rate, debris size and the ease with which debris are expelled from the contact, and concluded that the fillers interrupt the formation of the larger debris that form during severe wear of PTFE.

17.1.4 PTFE-based nanocomposites

In practice, PTFE microcomposites are loaded with more than 20% (by volume) filler and because the fillers are inherently hard and wear-resistant, abrasion to the counterface can be problematic. Nanoparticles are of the same size scale as counterface asperities and therefore have potential as wear-resistant, nonabrasive fillers. In addition, nanocomposites can have tremendous particle number densities and surface areas with low filler fractions ($<10\%$) of nanoparticles. In various other polymeric systems, low filler fractions of nanoparticles have resulted in impressive improvements in mechanical properties such as strength, modulus and strain to failure [24–27].

In 1996, Wang et al. demonstrated the potential benefits of nanoparticles in tribology using a polyetheretherketone (PEEK) matrix [28–32]. PEEK nanocomposites had optimal wear rates with roughly 2–4% filler fractions of nanoscale ZrO_2, Si_3N_4 and SiO_2 [28–30]. Later experiments with nanoscale SiC showed optimal wear performance at 1% filler fraction [31]. They also demonstrated the superior wear and friction performance of a 10 wt% SiC nanocomposite over 10 wt% SiC micrometer particle and whisker-filled PEEK composites [32]. In all cases, the improvements in friction and wear of the nanocomposite samples were attributed to the tenacity and uniformity of the protective transfer films.

Despite the success of microfillers in abating severe wear of PTFE and the demonstrated benefits of nanoparticles on the properties of other polymer matrices, conventional wisdom suggested that nanoscopic fillers would be ineffective in reducing the wear of PTFE. Tanaka and Kawakami [18] found evidence in support of this in a study varying the filler in a PTFE matrix. They found that the sub-micrometer hard particle-filled composite had poor wear resistance compared to the larger hard particle-filled composites in the study, and concluded that fillers must be of sufficient size to be effective. They suggested that sub-micrometer fillers were unable to prevent transfer and large-scale destruction because they were simply swept away within the matrix during plowing by relatively large counterface asperities.

In 2001, Li et al. [33] filled PTFE with nanoscale ZnO, and found 15 wt% to be the optimal filler fraction for wear resistance while retaining a low coefficient of friction. Chen et al. [34] created a PTFE nanocomposite with single-walled carbon-nanotubes and found that friction coefficient was reduced slightly and wear resistance was improved by more than two orders of magnitude over unfilled PTFE. Sawyer et al. [35] made nanocomposites of PTFE with 38 nm Al_2O_3 and found a 600X reduction in wear with 20 wt% filler concentration. Wear was reduced monotonically as filler concentration was increased to 20 wt%. While similar improvements in wear resistance were found by Burris and Sawyer

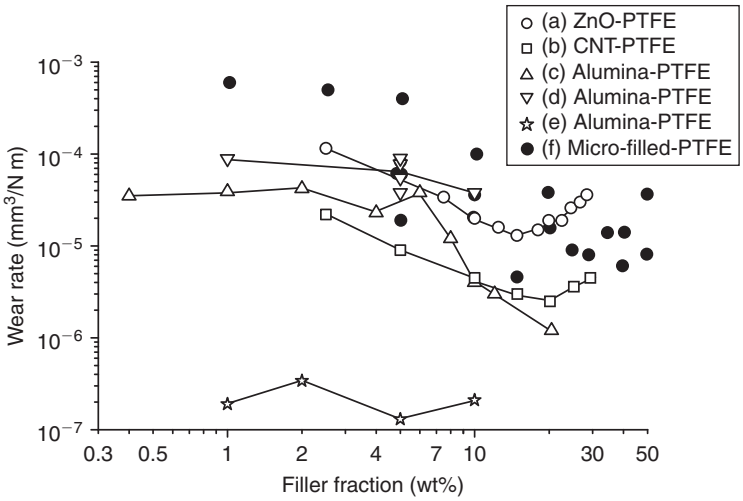

Fig. 17.2. Wear rate plotted versus filler fraction for the PTFE nanocomposites in the tribology literature. The microcomposites from Fig. 17.1 are shown collectively in Fig. 17.2 as filled circles. Data sets are listed as a–f: (a) Li et al. (2001), (b) Chen et al. (2003), (c) Sawyer et al. (2003), (d) Burris and Sawyer (2005), (e) Burris and Sawyer (2006), (f) see Fig. 17.1. Nanocomposites can have substantially improved wear rates at filler fractions below 10 wt%, but show a large degree of variability between studies.

using 44 nm alumina nanoparticles of the same phase (70:30 Δ:Γ) [36], the use of 80 nm α phase alumina was found to reduce wear by an additional 100X [37]; it was hypothesized that an irregular particle shape was responsible for the vast improvement in tribological performance.

Figure 17.2 shows wear rate plotted versus filler fraction for the PTFE nanocomposites in the literature. In general, microcomposites are optimized at higher filler fractions, while nanocomposites are optimized at lower filler fractions. With as little as 0.4 wt% filler fraction of nanoparticles, wear rate can be reduced by a factor of 10, while negligible reductions in wear are observed with less than 5 wt% filler fraction of microparticles. Additionally, the wear rate of PTFE with low filler fractions of nanoparticles can have improved wear resistance over even highly reinforced microcomposites (10^{-7} mm^3/N m at 1 wt% versus 10^{-5} mm^3/N m at 50 wt%).

Initial rules of mixtures and preferential load support models of wear resistance have been inadequate to predict the success of nanofillers at low filler fractions. Early investigations of the dominant wear reduction mechanisms in PTFE nanocomposites focused on strengthening and toughening of the matrix and the transfer films. Li et al. [33] used scanning electron microscopy (SEM) to study cross-sections of unfilled and nanofilled PTFE. The neat PTFE had many fibers drawn from the bulk while the nanocomposite did not. They suggested that the nanoparticles effectively prevented the destruction of the banded structure. They also found thick, patchy transfer films formed by unfilled PTFE, while thin, tenacious transfer films were formed by the wear-resistant nanocomposite. It was offered that the nanoparticles help bond the transfer film to the counterface which promotes low wear by protecting the soft composite from direct asperity damage. Chen et al. [34] also found evidence to suggest that the nanotubes prevented destruction of the crystalline structure of the PTFE. The high aspect ratio fillers were thought to reinforce the matrix by intertwining with PTFE crystals. In addition, they hypothesized that the nanotubes may provide additional self-lubrication after breaking off from the composite during wear. In the study by Sawyer et al. [35], SEM revealed that the PTFE particles were decorated by the nanoscopic alumina during a powder-blending process that preceded compression molding. The resulting structure after molding was cellular with thin regions of highly concentrated alumina-rich

material surrounding micrometer-sized domains of nominally unfilled PTFE. These concentrated regions were hypothesized to act as barriers to crack propagation, reducing the delamination wear of PTFE. Further, it was offered that with increasing filler concentration, the number, size and possibly strength of the compartmentalizing regions increased.

In general, the results from the polymer nanocomposites tribology literature are striking. Contrary to early suggestions, the use of nanoparticle fillers in PTFE has been very successful with 1,000X improvements in wear resistance occurring with as little as 1 wt% nanoscale filler. Unfortunately, the literature is seemingly inconsistent with wear rates between studies varying by as much as 1,000X for a given filler fraction. With the large number of variables between studies and the qualitative descriptions of transfer films, debris morphology, mechanical properties and most importantly nanoparticle dispersion, it is difficult to identify the sources of the inconsistency which makes global statements about wear resistance mechanisms difficult. Previous studies suggest that the wear rates of these systems are complex and coupled, possibly involving crack deflection, filler/matrix interactions, regulation of debris size and debris/counterface interactions, but there is a current need for more quantitative measurements to enable application-specific system design. The following studies represent the beginning of an effort to clarify some of the underlying mechanisms that govern the tribology of PTFE nanocomposite systems. The first studies directly examine the effects of filler particle size in PTFE composites. The following studies quantitatively examine the morphological, tribological, compositional and chemical properties of the transfer films and address their influences on the tribosystem. The next series of studies investigates the nature of the matrix/filler interface and its effect on the tribology of the system. The final studies discussed focus on the phase and morphology changes in the PTFE that occur as a result of nanoparticle inclusion, and the effects of these changes on the tribosystem.

17.2 Current and Ongoing Studies

17.2.1 Investigations of particle size

The hypothesis that filler particles must be of sufficient size to effectively provide wear resistance to PTFE was founded on the observation of wear rates of sub-micrometer (0.3 μm) TiO_2-filled composites exceeding those using fillers at sizes of several micrometers or more of materials such as chopped glass fibers, bronze and ZrO_2 [18]. In that study, however, each filler material was tested at a single particle size, thus the effect of filler particle size was not isolated from any possible effect of filler material type. Despite wearing more rapidly than the glass, bronze and ZrO_2–filled composites, the sub-micrometer TiO_2 fillers in several instances did in fact provide wear rate reductions of two-orders-of-magnitude compared to unfilled PTFE and no clear evidence is provided that larger TiO_2 fillers would have augmented this wear resistance any further. Li et al. [33] demonstrated the ability of nanofillers to provide wear resistance to PTFE with 50 nm ZnO particles reducing wear rate by nearly 100-fold in some cases. However, no micrometer-scale ZnO was included as a control to quantify this effectiveness relative to larger filler particle sizes. In their demonstration of the ability of an 80 nm alumina filler to provide PTFE wear resistance, Burris and Sawyer [36] also included a 0.5 μm filler for comparison, however this study still lacked a control within the range from several micrometers to approximately 30 μm conventionally deemed suitable for PTFE wear resistance [18].

To more clearly assess effects of filler size on PTFE wear resistance, a study [38] was performed using two alumina nanofillers of size 40 nm (27–43 nm) and 80 nm, as well as four alumina microfillers of size 0.5 μm (0.35–0.49 μm), 1 μm, 2 μm (0.9–2.2 μm) and 20 μm, all being provided by the same commercial manufacturer and being of the same α phase. In some cases the manufacturer specified a particle size range, indicated parenthetically. Each alumina particle type was blended at 5 wt% into commercially available PTFE powder of ~30 μm particle size using a Hauschild mixer, with the powder mixture being cold-pressed at 40 MPa into a cylindrical preform which was sintered in nitrogen

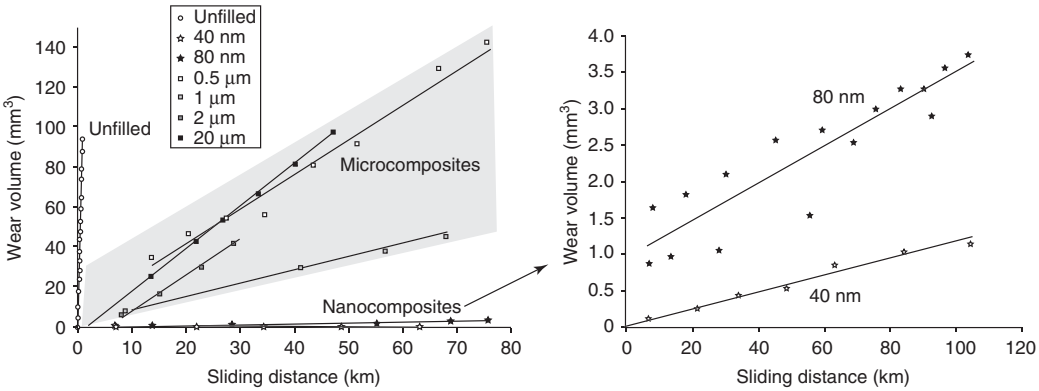

Fig. 17.3. Wear records for unfilled PTFE as well as for PTFE micro- and nanocomposites incorporating α phase alumina filler particles at 5 wt%. While the microcomposites fall within a diagonal band, an inset is provided with a magnified wear volume axis so that the low levels of nanocomposite wear may be seen.

at 360 °C. Composite pin specimens (4 mm × 4 mm cross-section) were machined from the sintered preforms, and tested in sliding contact with 304 stainless steel counterfaces ($R_a = 0.05\,\mu$m) in air at room temperature. Intermittent pin mass loss measurements were used to quantify composite wear.

The evolution of wear with increasing sliding distance for composite pins produced using a commercial G580 PTFE resin is plotted in Fig. 17.3. These tests were conducted in unidirectional sliding contact on a three-pin-on-disk tribometer at a sliding speed of 10 mm/s and a contact pressure of 3.1 MPa. As expected, unfilled PTFE wore so rapidly, losing nearly 100 mm^3 of wear volume within 1 km of sliding distance, that it falls very tight to the vertical axis. In contrast, the two nanocomposites wore so slowly, requiring sliding distances in excess of 100 km to reach wear volumes on the order of a couple cubic millimeters, that their wear records fall very tight to the horizontal axis. An inset is provided expanding this portion of the plot, so that the nanocomposite wear behaviors may be more clearly seen. The four microcomposites fall within a diagonal band across the plot, clearly providing unfilled PTFE an increase in the wear resistance, though far less than the wear resistance provided by the superior nanocomposites.

At steady state under constant load, the volume loss increases in proportion to the sliding distance such that for each composite a steady state wear rate is quantified and plotted as a function of filler particle size in Fig. 17.4. As compared to the unfilled PTFE value near 0.7×10^{-3} mm^3/N m, the microcomposites each provided wear reductions of nearly two-orders-of-magnitude, with wear rates falling closer to 10^{-5} mm^3/N m. The two nanocomposites provided an additional two-orders-of-magnitude decrease in wear rate, with wear rates near 10^{-7} mm^3/N m. The wear behavior as a function of filler particle size was also duplicated in a series of composites produced using an alternate (7C) commercial PTFE grade, not only in the same unidirectional three-pin-on-disk tribometer but also under oscillatory sliding contact against the polished 304 stainless steel at the same contact pressure and speed using a stroke length of 45 mm [39]. Despite drastically altering the wear behavior of PTFE, the alumina filler particles had little effect on the friction coefficient as the filled and unfilled PTFE all had measured friction coefficients of approximately $\mu = 0.18$ at the 10 mm/s test speed.

Following less than a kilometer of unidirectional sliding of unfilled PTFE, the countersurface was covered with abundant plate-like debris, while the microcomposites required 50 km or more to generate a comparable volume of characteristically finer debris. Despite being given more than 100 km of sliding distance, the nanocomposite wear debris were observed to be both fine and sparsely distributed about the wear track edges. SEM within the wear tracks (not shown) revealed that the microcomposites left abraded grooves and loosely bound debris on the stainless steel counterfaces. The nanocomposites were found not to cause such abrasion but instead left thin transfer films, and even though cracking

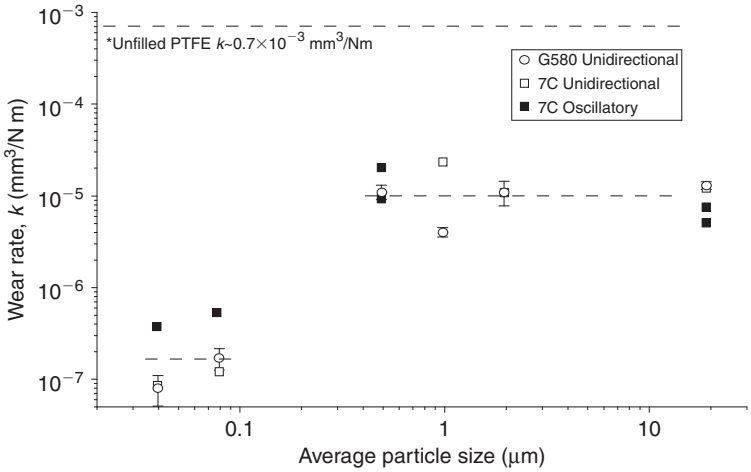

Fig. 17.4. Steady-state wear rate of alumina-filled PTFE composites as a function of filler particle size. Composites formed with either G580 or 7C resin and tested in either unidirectional or oscillatory (45 mm stroke length) sliding contact against 304 stainless steels. There is a two-order-of-magnitude reduction in wear rate from moderate wear to low wear as filler size is reduced from 0.5 μm to 80 nm.

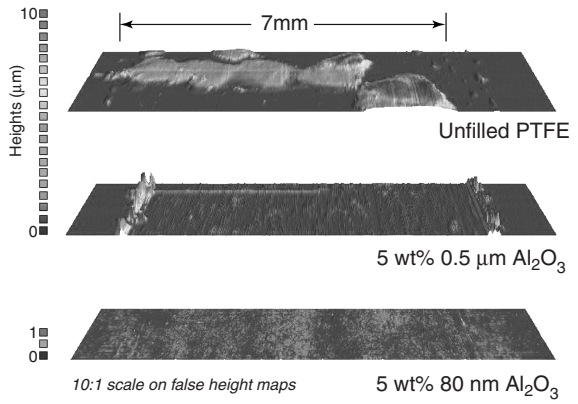

Fig. 17.5. Mapping stylus profilometry measurements of transfer films on polished counterfaces. Transfer film of unfilled PTFE (top), 5 wt% 500 nm α alumina-filled PTFE transfer film (center), 5 wt% 80 nm α alumina-filled PTFE (bottom). The stylus has a 12.5 μm diameter tip and measurements were made using a contacting force of 100 μN.

did appear in the thickest regions of these films, they appeared to remain coherent and well-adhered without liberating numerous transfer wear debris.

Clear differences in the transfer morphologies of unfilled, microfilled and nanofilled PTFE after oscillatory sliding can be observed in the mapping stylus profilometric transfer film measurements shown in Fig. 17.5. The unfilled PTFE transferred plates of material with characteristic in-plane dimensions of 1–2 mm and thicknesses of 5–10 μm. The microcomposite transferred substantially smaller platelets with in-plane dimensions of 100–200 μm and thicknesses of 0.5–2 μm. A comparable reduction in transfer size is obtained by replacing microparticles with nanoparticles. The transferred particles of nanocomposite material have in-plane dimensions of 20–50 μm and thicknesses of 50–500 nm.

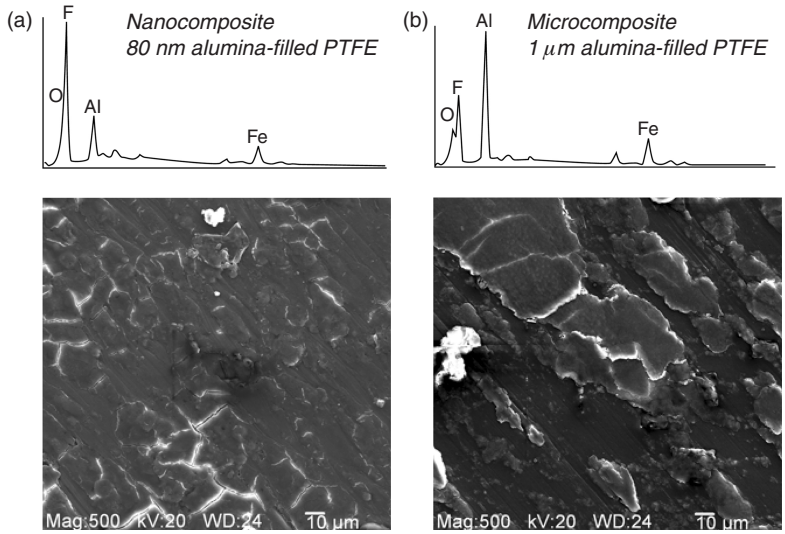

Fig. 17.6. Secondary electron images from example wear surfaces of a (a) nanocomposite (80 nm filled) and (b) microcomposite (1 μm filled). EDXS spectra from each are also provided, indicating F from the composite matrix, Al from the composite filler and Fe from debris abraded off the mating steel countersurface.

The SEM image from the nanocomposite pin specimen in Fig. 17.6 shows "mudflat" cracking throughout an otherwise smooth and coherent surface layer covering the worn pin. Higher magnification imaging (not shown) revealed that fibrillated PTFE spanned these cracks and appeared to stabilize the surface layer against breakdown and wear debris formation. In contrast, the worn microcomposite shows an incomplete flowing surface layer that appears to be flaky and less adherent, transforming into wear debris of larger size. Energy Dispersive X-Ray Spectra taken from these worn surfaces reveal Kα peaks at energies of 0.85, 1.49 and 6.40 keV, respectively for F from the PTFE matrix, Al from the alumina filler and Fe from steel particles abraded from the countersurface. Ratios of the heights of these Al and Fe peaks to the F matrix peak can serve as indicators of the relative amounts of alumina filler and steel wear debris upon the composite surface. For unworn composites at 5 wt% alumina, the Al/F ratio is observed to be approximately 0.2. After sliding, this ratio may increase as the filler accumulates at the near surface region due to preferential removal of the less wear-resistant PTFE matrix as previously reported for PTFE microcomposites [40]. Following testing, microcomposites were found to accumulate more filler at the surface with Al/F ratios ranging from 1 to 2, while the Al/F ratios of the nanocomposites never exceeded 0.5. Consistent with SEM observations of counterface abrasion, the Fe/F ratios of the microcomposites were greater than 0.2 (often well beyond 0.2) while those of the nanocomposites were less than 0.2. This difference is even more striking when one considers the extended sliding distances of the nanocomposite tests and the fact that the near surface material of the microcomposites, including the embedded steel from counterface abrasion, is removed at a rate 100 times greater than the near surface material of the nanocomposites.

An additional test program produced composites having a mixture of nanoparticles (40 nm) and microparticles (20 μm), so that comparison of the wear behaviors to those of composites filled at 5 wt% with only nanoparticles or microparticles might elucidate predominating wear mechanisms. As shown in Fig. 17.7, these mixed-filler composites were produced either with 5 wt% of each filler, or with 2.5 wt% of each. In either case, the mixed-filler composites displayed wear rates more near to the 10^{-5} mm^3/N m microcomposite value than the 10^{-7} mm^3/N m nanocomposite value. It can be concluded that while microparticles interfere with the severe wear mechanisms that result in large debris and rapid wear of PTFE, they supplant the wear resistance offered by the nanoparticles by

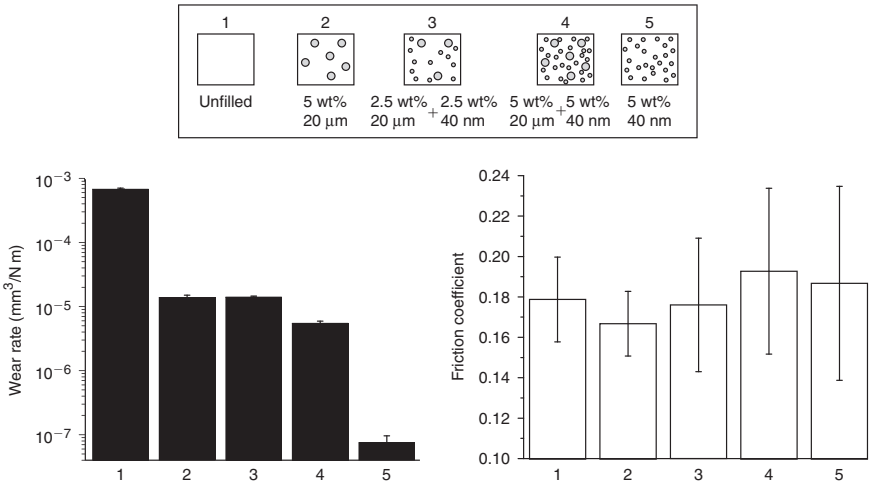

Fig. 17.7. Wear and friction behavior of five different PTFE composite materials sliding against 304 stainless steel, indicating the effect of inclusion of alumina microparticles (20 μm) and nanoparticles (40 nm), as well as mixtures of micro- and nanoparticles. The microparticles disrupt low wear by providing a wear pathway that is not otherwise available in the nanocomposite.

providing an otherwise unavailable wear pathway. Presuming the nanocomposite wear mechanism is one of transfer wear, where additional removal of nanocomposite material is activated to replenish detached and discarded transfer films, countersurface abrasion induced by the microparticles would increase wear rate by reducing the residence time of transfer material. Such a hypothesis would benefit from more focused transfer film investigations on microcomposites and nanocomposites.

17.2.2 Investigations of transfer films

Contrary to early suggestions that nanoparticles could not appreciably improve the wear resistance of PTFE, it has been shown that nanofillers can be far superior to microfillers with a transition in the dominant wear reduction mechanism occurring at a particle size approaching 100 nm. Preliminary evidence suggests that reduced counterface abrasion, third body wear and retention of protective transfer films are primarily responsible for the improvements in wear resistance. Thin, uniform transfer films consistently accompany wear resistance in the tribological nanocomposites literature [28–30, 33, 36, 37, 41, 42], but quantitative measurements of these films are lacking. Some authors suggest that wear resistance of the nanocomposite is due to protection from the transfer film while others offer that the films are formed as a consequence of low wear. It is currently unclear why and how these films form, how they facilitate wear resistance, if they are composed primarily of the PTFE, the filler or the composite, and if chemical reactions are involved.

Burris and Sawyer [36] conducted a study with 5 wt% α phase and Δ:Γ phase alumina-PTFE nanocomposites against various rough counterfaces to study the effect of asperity size on the transfer and wear of different PTFE nanocomposites. The surfaces were made using different standard finishing techniques and interferometry measurements of these surfaces are shown in Fig. 17.8.

Wear rates for these composites are plotted versus counterface roughness R_q in Fig. 17.9. The different phases of alumina were found to result in widely different tribological properties despite identical processing and testing. Wear rates of Δ:Γ alumina nanocomposites increased monotonically ranging 50–300 $\times$ 10^{-6} mm^3/N m with increased surface roughness. Additionally, wear debris were relatively large and transfer films thick and discontinuous. Wear rates of α alumina nanocomposites did

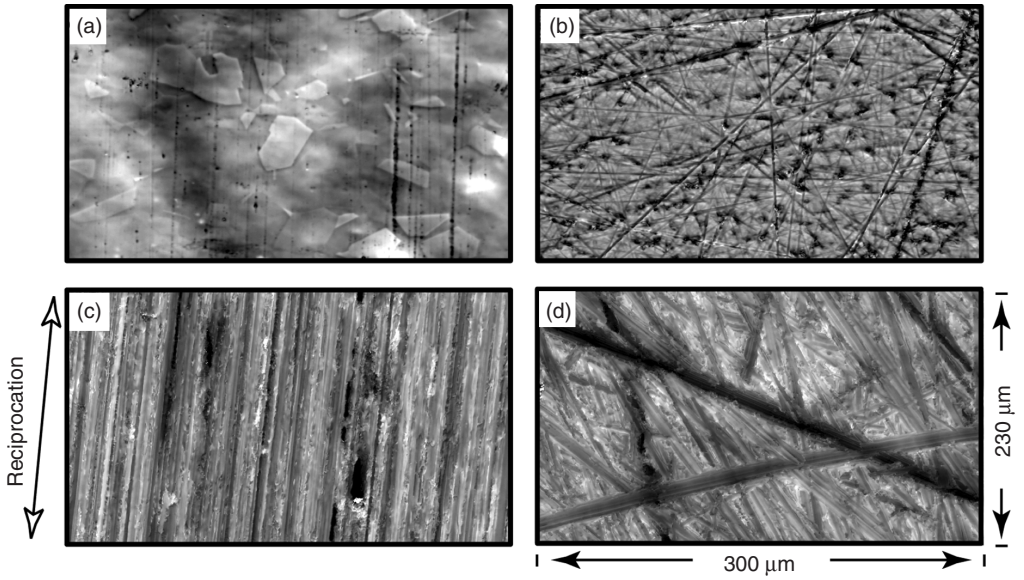

Fig. 17.8. Surfaces used to study roughness effects on PTFE nanocomposite transfer and wear: (a) electro-polished – Rq (root mean squared roughness) = 80 nm, (b) lapped – Rq = 160 nm, (c) wet-sanded – Rq = 390 nm and (d) dry-sanded – Rq = 580 nm. Note that the lay of the wet-sanded surface is oriented in the direction of sliding; it is smoother in the direction of sliding than against it.

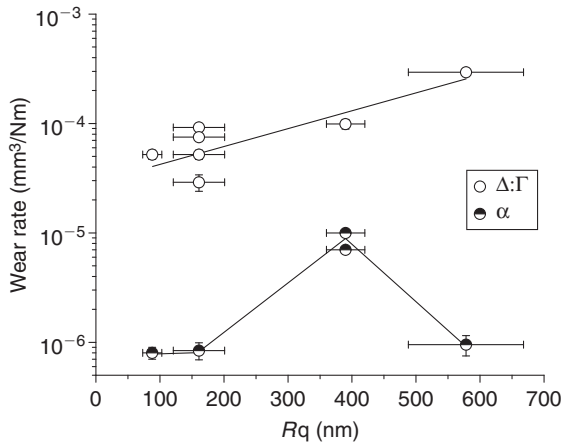

Fig. 17.9. Wear rate plotted versus counterface surface roughness, R_q for 5 wt% 40 nm Δ:Γ phase and 80 nm α phase alumina-PTFE nanocomposites. The two phases of alumina filler produce wear rates that differ by 100X on average with different surface sensitivities.

not correlate with roughness and were significantly lower than those of the Δ:Γ nanocomposites ranging from $0.8^{-10} \times 10^{-6}$ mm^3/N m. Wear rates from tests conducted on counterfaces without predominant orientation were equivalently low despite roughness ranging from 80 to 580 nm R_q. Transfer films on these surfaces were all thin and uniform. Testing against the oriented wet-sanded surface on the contrary increased the wear rate of the nanocomposites by an order of magnitude. A repeat at this condition

confirmed the validity of the result. Transfer films on the wet-sanded surface were incomplete, thick and banded in the direction of sliding [36].

17.2.2.1 Transfer film morphology

An examination of the data collected throughout the test reveals an additional key difference between Δ:Γ and α phase alumina nanocomposites. The Δ:Γ nanocomposites reached steady state almost immediately, while the α nanocomposites had a significant transient period of moderate wear followed by a transition to a lower steady state wear rate. Despite the relative insensitivity of steady state wear rates to counterface roughness for α nanocomposites, the transient wear rate during transfer film development increased monotonically with increased roughness. This is intuitive since larger asperities tend to remove more material during wear events. Additionally, the total volume removed during the transient portion of the test increases with increased roughness. These results suggest that as material is removed from the sample and deposited onto the counterface, more of the asperities become covered and the wear rate is reduced. Larger asperities require more material to transfer before steady state is reached, but at steady state, abrasion is insignificant and wear rate is independent of roughness. The orientation of the wet-sanded surface likely disrupted the formation of a stable transfer film, resulting in comparable transient and steady state wear rates. It can be concluded that the presence of a protective transfer film is necessary for low wear of PTFE nanocomposites. It is also interesting to note that when neither composite was sufficiently protected by transfer films, either during the transient region or against the wet-sanded surface, the α alumina nanocomposites outperformed the Δ:Γ nanocomposites. This suggests a difference in the wear mechanisms, which likely governs the ability of the composite to form protective films during sliding. Qualitatively, transfer films were found to increase in thickness and discontinuity with increasing wear rate.

Thin, uniform transfer films and fine debris consistently accompany wear resistance in these studies and in the nanocomposites tribology literature. Global relationships between wear rates and transfer films were studied by quantitatively measuring transfer films of widely varying PTFE-based tribosystems using either scanning white-light interferometry or mapping stylus profilometry. These systems include 5 wt% alumina-PTFE composites with μ and Δ:Γ particle phases, 40 nm, 80 nm and 0.5 μm particle sizes, and counterfaces of polished, lapped, wet-sanded and dry-sanded surface finishes. Wear rate is plotted as a function of maximum transfer film thickness in Fig. 17.10. Despite varying particle phase, size and surface finish, wear rate is approximately proportional to the maximum thickness of the transfer film cubed. Not only do thicker films imply larger debris, but it is suggested that thick transfer films are more easily removed by the passing pin, and as a consequence, need more rapid replenishment.

It is well known that under certain low-speed sliding conditions, PTFE deposits very thin and oriented transfer films [3, 43–47]. The orientation is thought to produce a model sliding condition where chain entanglement is minimized and pure axial sliding of PTFE chains past one another results in the very low friction coefficients observed under these conditions ($\mu = 0.03$–0.07). It is hypothesized that the role of the filler is to reduce gross damage to PTFE under severe sliding conditions, facilitating the formation of thin and aligned PTFE films, and enabling low wear of the nanocomposite.

The friction and wear properties of the films themselves were measured using microtribometry to test the hypothesis that thin, aligned films of unfilled PTFE are wear-resistant. Model films of PTFE were deposited onto a thin steel foil with a sliding velocity of 254 μm/s for 1,000 reciprocation cycles at 25 °C under 6.3 MPa of normal pressure. Atomic force microscopy (AFM) was used to estimate an average film thickness of 50 nm. After creation, the film-covered foils were cut into rectangular samples for testing. Custom-designed sample mounts fixed opposing foils into a crossed-cylinder geometry. This geometry reduces misalignment sensitivity, minimizes edge effects and helps reduce pressures to values more typical of those found in macroscale testing. Parallel (chains oriented in the direction of sliding) and perpendicular (chains oriented against the direction of sliding) aligned films were tested to study the hypothesized tribological anisotropy of aligned PTFE films. Normal and friction forces

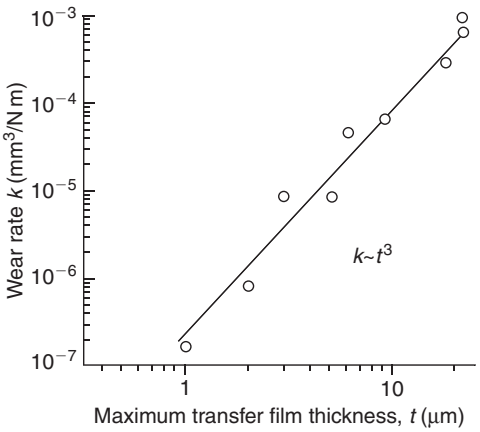

Fig. 17.10. Wear rate plotted versus the maximum transfer film thickness as measured with optical interferometry. This data includes results of 5 wt% 44 nm Δ:Γ, 80 nm α and 0.5 μm α composites against the best and worst performing counterfaces, and 5 wt% 80 nm and 0.5 μm composites and unfilled PTFE against polished surfaces. Wear rate is proportional to the maximum transfer film thickness cubed.

were continuously measured at the stationary pin, while a 600 μm reciprocation displacement was imposed on the counterface. Tests with an average sliding speed of 100 μm/s and a normal load of 500 mN were conducted over 250 sliding cycles. The contact patch was estimated with ex-situ optical observation to be 200 μm in diameter; this translates into an average pressure of 15 MPa. The results of the microtribometry experiments are shown in Fig. 17.11.

In line with the hypothesis that orientation in the sliding direction facilitates low friction and wear, perpendicular alignment of the films led to complete failure of the film (denoted by $\mu > 0.2$) in approximately 10 cycles, while parallel aligned films were at least 10X more wear-resistant. Despite having similar average values of friction coefficient for the first few passes, differences can be seen in the positionally resolved friction data as shown in Fig. 17.11(c) and (d). Examining the first pass, the parallel sample has a steady friction loop, while the perpendicular friction loop has significant scatter. The mechanism of motion accommodation appears more damaging in the case of the perpendicularly aligned films, and the tendency of these films to reorient into the direction of sliding is likely responsible for the erratic friction and wear behavior. The parallel aligned films have much lower wear presumably as a result of the stable orientation.

Since protective transfer films are necessary to reduce wear of these nanocomposites against counterface asperities, the wear rate of the transfer film places a lower limit on the wear rate of the composite. An estimate of wear rate for the parallel aligned films was calculated to determine whether model films of unfilled PTFE could possibly support low wear sliding. The contact area on the top foil (pin) and bottom foil (counterface) are 0.033 and 0.12 mm^2, respectively, so failure of the top film should occur first, followed by direct asperity contact and rapid deterioration of the bottom film. Failure of the top film in parallel alignment occurred after approximately 150 cycles. The wear rate in this case is calculated as

$$k = \frac{50 \times 10^{-6}\,\text{mm}}{15\,\text{N/mm}^2 \times 150\text{cycles} \times 1.2 \times 10^{-3}\,\text{m/cycle}} = 2 \times 10^{-5}\,\frac{\text{mm}^3}{\text{Nm}} \tag{17.1}$$

Despite the superiority of the parallel aligned transfer film, estimation of the wear rate reveals that rates are still orders of magnitude higher than those found for many low wear PTFE nanocomposites ($\sim 10^{-5}$ versus 10^{-7} mm^3/N m). It can be concluded that even model thin and aligned transfer films of

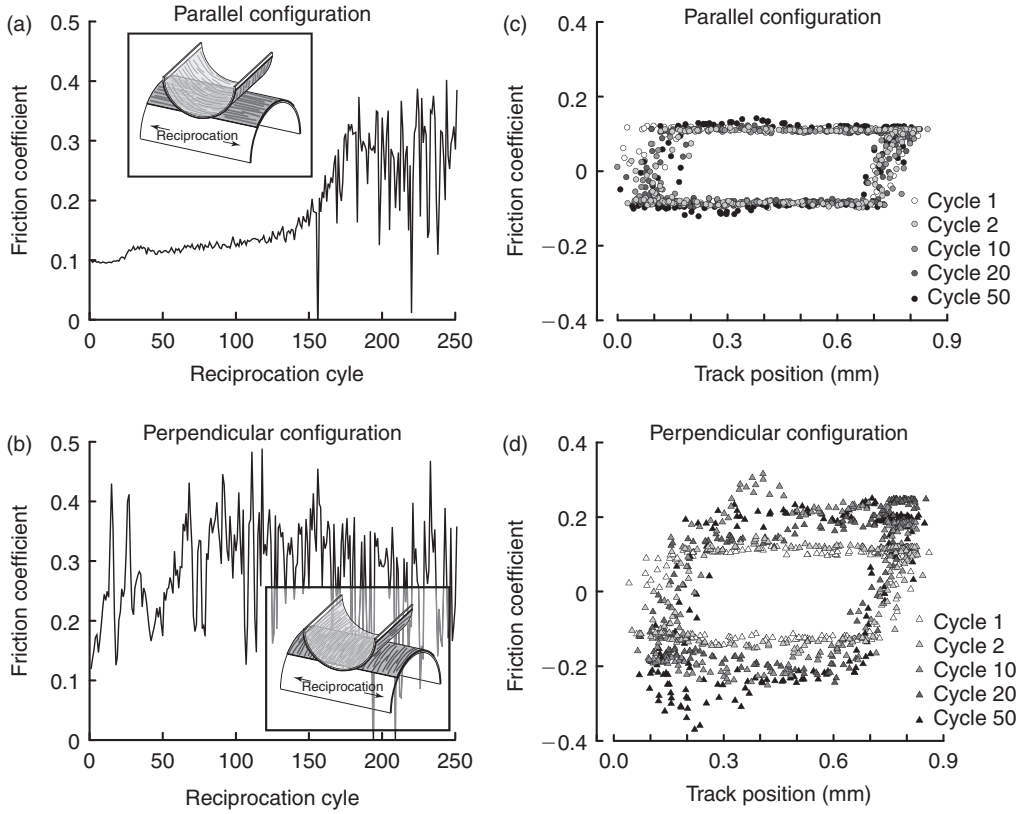

Fig. 17.11. Microtribometry friction results for the crossed cylinder-oriented PTFE transfer film tests. Friction coefficient is examined versus reciprocation cycle for (a) parallel and (b) perpendicular configuration. The evolution of friction coefficient along the reciprocation track is also plotted for both the (c) parallel and (d) perpendicular configurations. The perpendicular alignment of the films leads to rapid failure of the films due to a tendency to reorient during unidirectional sliding.

PTFE are incapable of supporting low wear sliding. The films formed by sliding of a low wear nanocomposite must therefore be comprised of composite material or some more wear-resistant variant of PTFE.

Similar experiments were conducted for transfer films of a low wear 10 wt% PEEK-filled PTFE composite. In each configuration, the composite film had lower and more stable friction coefficients for the duration of 1,000 cycle tests with no obvious signs of wear in post-test analysis. Clearly, the compositions and chemistries of these films are additional factors that require quantification for a more complete understanding of these nanocomposite systems.

17.2.2.2 Transfer film composition

Though X-Ray photoelectron spectroscopic (XPS) chemical and compositional analyses of unfilled polymer and microcomposite transfer films have been conducted by several investigators [20–22], it is unclear how composition and chemistry evolve in the transfer films of PTFE nanocomposites or how this evolution influences tribological phenomena observed during testing. XPS was used to test the hypothesis that transfer films consist of composite material. PTFE nanocomposites were created with 1/8%, 1/2 % and 1% filler fractions of 40 nm α alumina nanoparticles. In a control set, the particles were untreated and in a second set of samples, the nanoparticles were treated with a fluorinated silane. The treatment was hypothesized to improve dispersibility and compatibility with the matrix. Treated

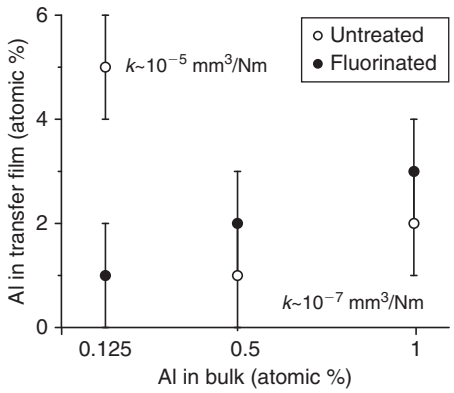

Fig. 17.12. Aluminum atomic content (%) in the transfer films of virgin and fluorinated nanocomposites plotted versus the atomic content as prepared in the bulk. Measurements were made in the center of each wear track. In low wear samples the aluminum content in the transfer film is linearly proportional to the aluminum content in the bulk sample. Evidence of filler accumulation was observed for the less wear-resistant sample.

(fluorinated) and untreated samples were compression molded, machined and tested. The tribological experiments were conducted on a linear reciprocating tribometer; the pin passes back and forth across a linear wear track. Photoelectron spectra of the C, O, F, Al and Si regions were collected using a PHI 5700 X-Ray photoelectron spectrometer equipped with a monochromatic Al Kα X-Ray source ($h\nu = 1486.7$ eV) incident at 90 ° relative to the axis of a hemispherical analyzer. The spectrometer was operated at high resolution with a pass energy of 23.5 eV, a photoelectron take off angle of 45 ° from the surface normal and an analyzer spot diameter of 1.1 mm. All spectra were collected at room temperature with a base pressure of 1×10^{-9} torr. Electron binding energies were calibrated with respect to the C1s line at 291.6 eV (C–F).

Even at very low filler fractions, alumina was found to transfer to the counterface with the PTFE (trace amounts of Si were also found in fluorinated samples). The atomic fraction of aluminum in the transfer films is plotted versus the aluminum content in the bulk in Fig. 17.12. Aluminum in the transfer films of fluorinated samples (filled circles) was found in direct proportion to the filler fraction in the bulk sample. The untreated 1/8% sample had an unexpectedly high amount of aluminum in the film, possibly due to poor dispersion or agglomeration during processing. Alternatively, aluminum could have accumulated in the transfer film with wear of the sample – this sample had 50X higher wear than any of the other samples – Blanchet and Han [40, 48] previously described this mechanism as one of preferential removal of PTFE from the system which leaves the interface rich with filler.

Similar XPS analyses of transfer films formed from both types of alumina particles revealed a higher proportion of oxygen than would otherwise be predicted based on the aluminum present, suggesting tribo-chemical oxidation of the PTFE during extended sliding. Furthermore, these measurements demonstrate a correlation between friction coefficient and the oxygen content of the transfer film (Fig. 17.13). It is unclear whether an increase in friction of the fully formed transfer film drives the oxidation or if oxidation itself, occurring in the creation of the transfer films, leads to the higher friction coefficients.

The transfer films formed from PTFE nanocomposites containing fluorinated alumina exhibited frictional behavior uncharacteristic of PTFE; friction coefficients were lowest at the reversals (ends of the wear track) and highest in the center. Based on this behavior and the oxygen-friction coefficient correlation presented earlier, it was hypothesized that oxygen content should decrease toward the ends of the wear track where friction was found to be lowest. Figure 17. 14 shows friction coefficient, transfer film thickness and oxygen content as functions of the pin center track position over half of the track for a 2 wt% fluorinated 40 nm α phase alumina-PTFE nanocomposite. XPS was used to determine oxygen

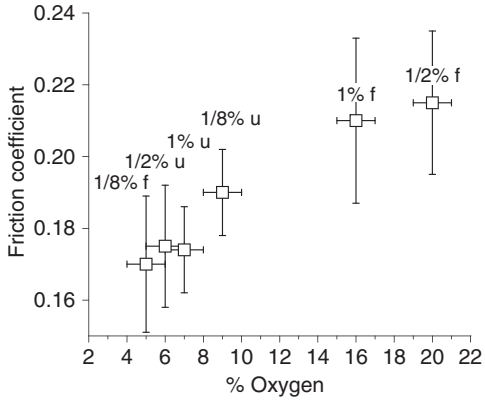

Fig. 17.13. Friction coefficient plotted versus oxygen content as measured using X-Ray photoelectron spectroscopy. The symbol "u" denotes untreated alumina and "f" denoted fluorinated alumina.

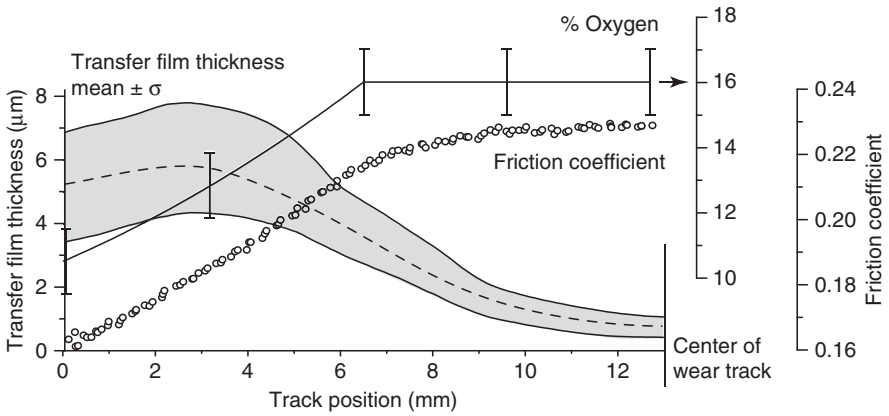

Fig. 17.14. Transfer film thickness, oxygen content and friction coefficient plotted versus track position over half of the wear track for a 1% fluorinated sample. The transfer film thickness envelope represents the mean plus and minus one standard deviation. The position-dependent friction coefficient correlates well with both oxygen content and thickness.

content in the films and three-dimensional mapping stylus profilometry was used to map film thickness; the thickness envelope shown in Fig. 17.14 reflects averaged results of mapping stylus profilometric measurements of the transfer film plus and minus one standard deviation. Both oxygen content and thickness correlate well with the friction coefficient along the wear track for the final cycle of sliding.

17.2.2.3 Transfer film chemistry

The oxidation of PTFE is initially surprising given its known chemical inertness. However, very wear-resistant materials produce very thin transfer films that are exposed to prolonged frictional energy dissipation at the interface. Over extended sliding distances, sufficient energy can be absorbed by these thin layers to initiate even low-probability chemical events. XPS analysis of a 5 wt% 80 nm α alumina transfer film after sliding with a wear rate of 10^{-7} mm^3/N m further probed the tribo-chemical degradation of low wear PTFE. The comparison of the core level C 1s spectra of unfilled PTFE

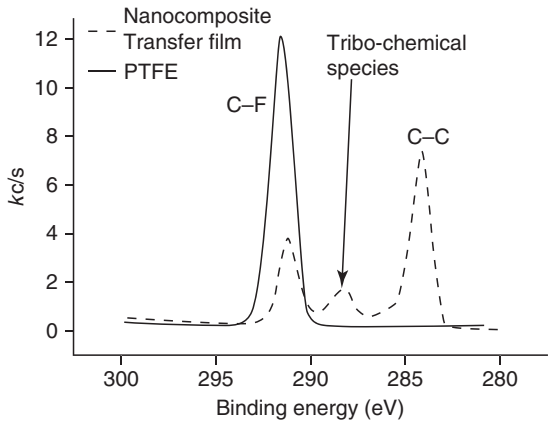

Fig. 17.15. Comparison of the core level C 1s spectra of unfilled PTFE to that of the nanocomposite transfer film. The appearance of a new peak at 288 eV provides evidence of a chemical transformation in the PTFE that occurs during wear.

to that of the nanocomposite transfer film shown in Fig. 17.15 demonstrates clear evidence of a chemical transformation of PTFE in the process of transfer film deposition and wear. The data confirm a reduction in C–F intensity at 292 eV, consistent with defluorination of the transfer film and the measured reduction in the F 1s integrated intensity (data not shown). This change is accompanied by the appearance of new C species giving rise to intensity at 288 and 284 eV. While the relative changes in the 292 and 284 eV regions could be rationalized through the adsorption/deposition of adventitious carbon during sliding or sample preparation, the 288 eV feature can be correlated with the relative wear resistance of filled PTFE transfer films. As such, we conclude that the formation of unique chemical species in these wear-resistant transfer films accompanies the relative changes in atomic concentration.

Several investigators have intentionally degraded PTFE using various techniques including gamma ray, electron beam and ultraviolet irradiation, and have correlated chemical degradation with changes in mechanical properties [49–52]. For example, Zhao et al. [53] noted a rapid fluorine loss on the surface of PTFE when exposed to vacuum ultraviolet radiation as well as increased optical absorbance due to carbon exposure, which resulted in a brownish appearance of the sample. Similar brown discolorations are often found in low wear transfer films. Lappan et al. [54–56] and Oshima et al. [57] used infrared spectroscopy to identify various reaction products from the degradation, noting processes involving defluorination and chain scission which produce terminal and branched CF_3 groups, C–C double bonds and branched (crosslinked) carbon structures. COF and COOH have also been observed. High-speed magic angle spinning (HS MAS) NMR spectroscopy measurements of degraded PTFE by Katoh et al. [58] and Fuchs et al. [59] provided evidence of crosslinking in degraded PTFE. Oshima et al. [57] used the HS MAS NMR data to identify chemical structures of CF_2, CF (crosslinking) and =CF (double-bonded carbon) in XPS spectra.

Blanchet et al. [11, 15, 60] previously conducted tribology experiments on irradiated PTFE and FEP composites and demonstrated that the wear resistance of each was improved by several orders of magnitude with 30 Mrad doses of electron irradiation. More recently, we conducted an analogous study to further explore the influence of degradation on the tribological properties of PTFE. A commercial chemical etch was used to emulate tribo-chemical degradation by stripping fluorine from the surface of an unfilled PTFE wear sample. Intensity at 288 eV was verified in the XPS spectrum of the etched surface. The tribological properties of the degraded PTFE surface coating were measured for linear reciprocating sliding at 6.3 MPa and 50 mm/s. The degraded PTFE was found to be 100X more wear-resistant than unfilled PTFE, verifying that conjugated PTFE offers the possibility of increased wear

resistance. But, a period of moderate wear was followed by a sharp increase in wear and a 10% reduction in friction coefficient as the more wear-resistant degraded surface wore through to the virgin PTFE beneath. The rate of material consumption due to wear here was greater than the rate of tribochemical degradation, and it is likely that in these nanocomposite systems, the degradation mechanism supplements the other more dominant mechanisms that enable degradation to occur.

17.2.2.4 Role of transfer films

It has been shown that transfer film morphology, composition and chemistry all play important roles in determining the wear rate of the films and thus the tribosystem. It has also been shown that certain surface characteristics can destabilize the transfer film which disables low wear sliding. It is clear that the presence of a high quality transfer film is a necessary condition for low wear sliding of PTFE nanocomposites; it is unclear whether it is a sufficient condition for low wear. To test this hypothesis, an alumina-PTFE nanocomposite known to ordinarily produce poor quality transfer films (5 wt% 44 nm Δ:Γ alumina) was tested upon a pre-deposited transfer film formed under ultra-low wear sliding conditions ($k < 10^{-8}$ mm^3/N m [61]). It was found that the composite had the same wear rate (7×10^{-5} mm^3/N m) whether it was tested against a wear-resistant transfer film or a fresh counterface. Despite the presence of an ultra-low wear transfer film, thick platelets indicative of delamination wear were deposited on top of the pre-existing transfer film. The abrasive wear that is reduced by the transfer film appears to have a negligible influence on the wear rate of this nanocomposite due to the severity of its delamination wear. In-situ optical microscopy of the wear track revealed that the transferred material is very unstable, moving appreciably after each cycle. Clearly the mechanics of the nanocomposite itself dominate the properties of this system and govern the development of the transfer film. These results suggest that while thin transfer films are required for low wear, they form as a result of the low wear debris morphology and are not themselves the source of wear resistance.

17.2.3 Investigations of internal interfaces

The critical role of transfer films in enabling low wear of PTFE nanocomposites has been demonstrated, but bulk properties of the composite seem to dictate the initiation and development of the films as well as the ability of the composite to achieve low wear against high quality transfer films. Bahadur and Tabor [23] and Blanchet and Kennedy [1] noted a trend of decreased wear debris size with decreased wear rate and suggested that the primary role of the filler was to reduce the size of the wear debris. Because the wear rate is proportional to volume, which is proportional to the cube of a characteristic diameter of the debris, reducing debris size inherently reduces the wear rate, promotes engagement of debris with the surface and improves transfer film stability. Burris and Sawyer [37] hypothesized that the size and shape of the debris during run-in were critical in the development of these transfer films, and that the film morphology observed during low wear was a consequence of low wear rather than the cause. They envisioned a wear model proposed by Blanchet and Kennedy [1], where the cracks that lead to the destructive delamination in PTFE were effectively arrested by the filler, resulting in reduced debris size and stable transfer film formation. The strength at the filler/matrix interface would have a critical influence on such a system.

Often, nanoparticles and polymer matrices are inert by design to limit environmental sensitivity of the tribological response. This inertness limits chemical interaction at the filler/matrix interface and can lead to inherent weakness. Wagner and Vaia [62] articulated the importance of the bonding at the interface for a nanotube-reinforced polymer. They calculated interfacial shear strength to be 3 MPa with only van der Waals interactions present, and in excess of 100 MPa with only 1% covalent bonding of the carbon atoms. Many investigators have successfully improved interfacial bonding in composites with surface coatings that compatibilize the filler with the matrix. He et al. [63] found improved mechanical properties and dispersion when the nanoparticles were plasma-modified, and Eitan et al. [25] found improved load transfer via strain-dependent Raman spectroscopy and improved bulk mechanical

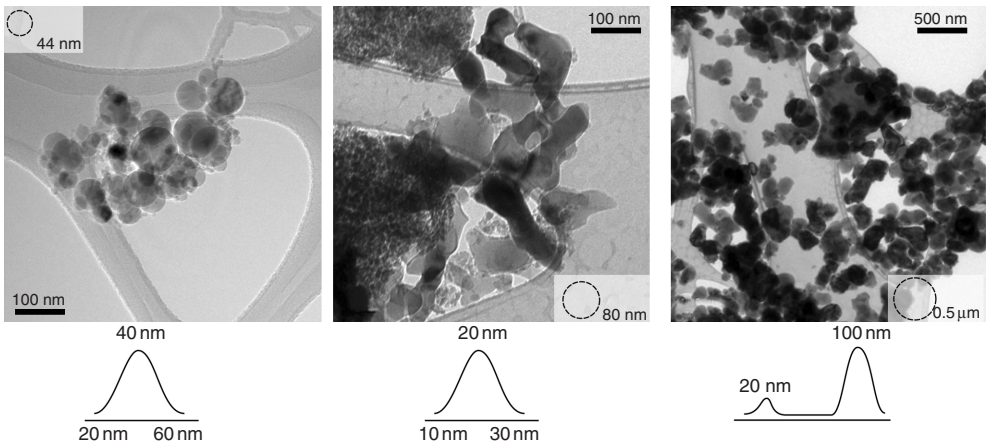

Fig. 17.16. Transmission electron images of 44 nm Δ:Γ (left), 40 nm α (center) and 80 nm α? (right) particles used in this study with size distributions estimated from TEM surveying.

properties of a treated MWCNT-filled polycarbonate over the nanocomposite with untreated nanotubes. While the studies of Burris and Sawyer [36, 37] showed a strong dependence of wear rate on alumina phase suggesting the potential importance of these internal interfaces in tribology, it was unclear whether observed differences were due to particle phase or size since both phase and size varied in the experiments. Recently, experiments were conducted on PTFE nanocomposites with smaller α phase alumina to evaluate the potential size effect. Figure 17.16 shows TEM images of the 44 nm Δ:Γ, 40 nm α and 80 nm α phase nanoparticles. The α phase particles have an irregular plate-like morphology while the Δ:Γ particles are spherical.

Tribological experiments were conducted on nanocomposites of these particles at various filler fractions against lapped 304 stainless steel counterfaces in standard laboratory conditions at 50 mm/s and 6.3 MPa of normal pressure. Wear rate is plotted versus alumina filler fraction in Fig. 17.17. The wear rates of the 40 and 80 nm α alumina-PTFE nanocomposites are insensitive to size and filler fraction in the range from 1/2–5% filler and these particles provide additional 100–1000X improvements in wear resistance over the Δ:Γ phase alumina-PTFE nanocomposites. It can be concluded that the differences in wear rates are not attributable to particle size, and although these dispersions have not yet been characterized, the difference is thought not to be due to dispersibility since the 40 nm α phase particles have higher specific surface area and were observed to agglomerate substantially more than the other particles during nanoparticle imaging. Though the wear reduction mechanism of the α phase particles remains unclear, it appears to be related to the nature of the interface.

It was hypothesized that additional gains in tribological performance could be achieved by compatibilizing the nanoparticles with the matrix. A nanoparticle surface fluorination was thought to not only provide compatibility with the matrix, but the decrease in nanoparticle surface energy due to the fluorination was thought to aid dispersion; poor dispersibility was suspected as the source of the unusual scatter in the 40 nm α nanocomposites. The 40 nm α phase particles were chemically treated with 3,3,3-trifluoropropyl trimethoxysilane. Infrared absorption spectroscopy confirmed the presence of the fluorinated groups and thermal gravimetric analysis was used to estimate the mass fraction at 3%. Nanocomposites with filler fractions of 1/8, 1/2 and 1% untreated and fluorinated nanoparticles were tested to investigate the effects of the interface treatment on the tribological properties of the nanocomposite. Wear volume is plotted versus the sliding distance on the left-hand side of Fig. 17.18. In general, the fluorinated samples were very well behaved in comparison to the untreated samples. Transients are steeper and longer lasting with more material removed for samples of lower nanoparticle filler fractions. The untreated alumina nanocomposites behaved erratically by comparison. Steady state wear

AQ1

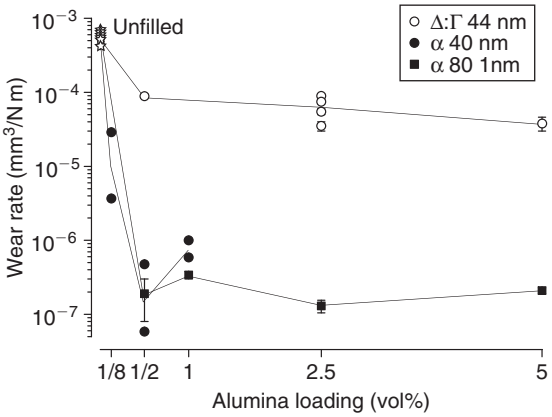

Fig. 17.17. Wear rate plotted versus filler fraction for alumina-PTFE nanocomposites with varying nanoparticle phase against a lapped counterface. Error bars represent the experimental standard uncertainty in the measurement of wear rate.

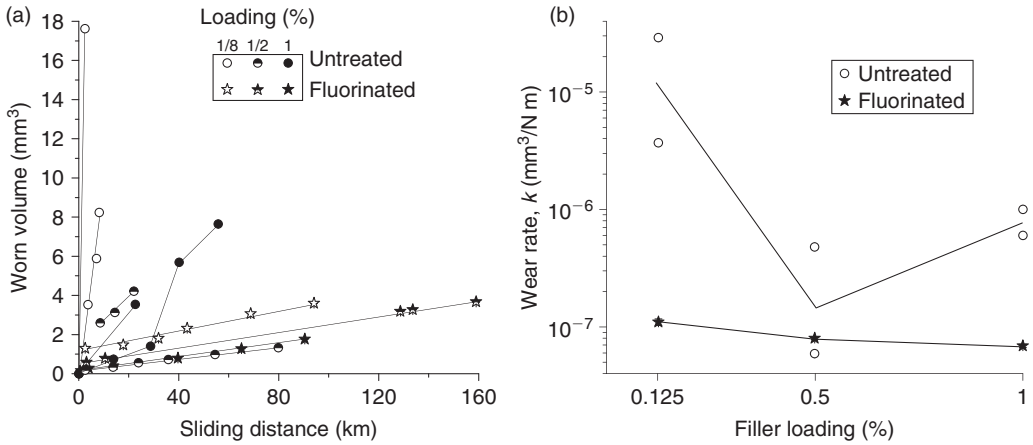

Fig. 17.18. (a) Worn volume plotted versus sliding distance for untreated and fluorinated 40 nm α phase alumina-filled PTFE. (b) Wear rate plotted versus filler fraction for untreated and fluorinated 40 nm α phase alumina-filled PTFE. Linear reciprocation experiments were conducted against lapped 304 stainless steel counterfaces under standard laboratory conditions with a normal load of 250 N.

rates are plotted versus filler fraction in Fig. 17.18. The large sample to sample variation of the untreated nanocomposites is clear with the low wt% samples having nearly an order-of-magnitude difference in wear rates of identically prepared samples. The wear rates of the functional nanocomposites differ by less than 2X from 1/8% to 1%, and decrease linearly with increasing filler fraction; variations in wear rates of 2X or less for PTFE nanocomposites are rare even for sample-to-sample variations. With the addition of 1/8% functional nanoparticles, the wear resistance of PTFE was improved by over 5,000X. It is unclear whether the variations in wear rates were dominated by dispersion, interface strength or both. Efforts to interrogate and quantify dispersions are currently underway.

AQ2

17.2.4 Investigations of matrix phase and morphology

Previous studies have shown that subtle changes, such as nanoparticle shape, phase and surface chemistry, can have dramatic effects on the wear rate of the PTFE nanocomposite. A previous hypothesis was that these factors increased the particle/matrix interface strength, but filler particle surfaces can also affect the local phase, morphology and mobility of the polymer chains at the interface. This layer of affected polymer in the vicinity of the particle is known as the interfacial region, interaction zone and interphase. We will refer to it as an interfacial region here. Owing to its characteristic nanometer size scale, it is often appropriately neglected in microcomposites. However, the interfacial region can often be comparable in thickness to nanoparticle fillers and can therefore dominate the properties of a nanocomposite. In amorphous polymers, the primary impact is on the chain morphology and mobility. Sternstein et al. [27, 64] did a systematic study of the particle/matrix interface strength effects on the rheology of nanocomposites and proposed a theory for reinforcement and nonlinear viscoelasticity of polymer nanocomposites that is based on the trapped entanglements of chains near the polymer/matrix interface and the consequent far-field effects on other polymer chains. Maiti and Bhowmick [65] used AFM to measure interfacial thickness, and found thickness of the region to increase with increased filler/matrix compatibility. Eitan et al. [25] observed a similar relationship for treated and untreated nanotubes in a polycarbonate matrix. Additionally, it was found that fracture occurred preferentially within the matrix itself rather than at the filler/matrix interface, suggesting that the interface and interfacial region can both be stronger than the unfilled polymer. The manifestations of interface effects in amorphous polymers have been observed by numerous researchers and include changes in glass transition temperature, modulus, toughness and rheology [24, 25, 27, 64, 66–69]. In semi-crystalline polymers, nanoparticles can alter the crystalline phase [70], morphology [71, 72] and the degree of crystallinity [73, 74], which can extend the influence of the nanoparticles. Such changes in crystalline morphology can have significant influences on mechanical behavior, but it is unclear whether such effects are present in PTFE nanocomposites or to what extent tribological properties are altered due to these effects. The role of crystallinity and crystal phase is explored in the following paragraphs.

PTFE is a semi-crystalline polymer known to have a complex molecular organization with three phases existing near room temperature at ambient pressure. Phase II [75–80] is typically stable below 19 °C, and is characterized by a triclinic unit cell with $a = b = 0.559$ nm and $\gamma = 119.3°$. The molecular conformation is described by Clark [75] as a noncommensurable 13/6 helix. As the temperature increases above 19 °C, phase IV becomes stable, the molecules untwist to a possibly commensurable 15/7 helix and the unit cell becomes hexagonal with a 1% increase in the lattice parameter ($a = b = 0.566$ nm) [75]; macroscopically, this results in an increase in volume [80]. Additionally, Kimmig et al. [81] noted a rapid increase in the density of coherent helical reversal defects possibly associated with the onset of helix commensurability. As the temperature increases above 30 °C, the hexagonal unit cell becomes distorted [82], the Bragg reflection at $2\theta = 42°$ broadens [83] and molecular disorder increases [77, 81, 84] as intramolecular forces begin to dominate intermolecular forces [81]. It has been suggested that molecular disorder increases with increased temperature because axial and rotational oscillations of molecules become more pronounced and helical reversal defects increase in length and become incoherent.

While it has been shown that the degree of crystallinity has a minimal role on the wear rate of PTFE [6, 85], phase and temperature have both been found to have dramatic influences on the mechanical and tribological properties of PTFE. Flom and Porile noted a dramatic effect of the phase of PTFE on its tribological properties [2]. They performed sliding experiments with self-mated PTFE at speeds of 11 and 1890 mm/s and found an abrupt and reversible increase in the friction coefficient as the background temperature increased above a threshold value near room temperature in both cases. They hypothesized that the increase was associated with the phase transition from II to IV at 19 °C. Steijn [5] also found increased friction coefficients as the temperature increased from 19 to 30 °C despite the more global trend of reduced friction coefficient with increased temperature. Makinson and Tabor [3] found

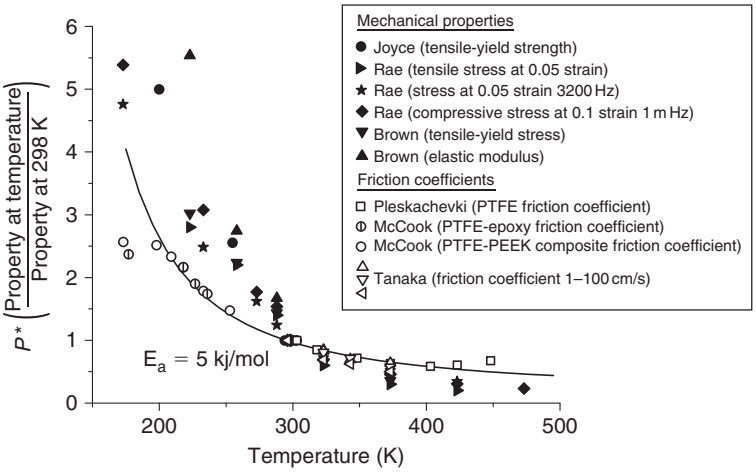

Fig. 17.19. Normalized properties plotted versus temperature for variable temperature studies available in the literature. The normalized property is defined as the ratio of the value at temperature to the room temperature value. Various tribological and mechanical experiments suggest that deformation of PTFE is a thermally activated process.

evidence of strong adhesion to the counterface and proposed a lamellar effect of intercrystalline shear governed by van der Waals interactions between polymer chains. Studies by Steijn [5], Tanaka et al. [6], Blanchet and Kennedy [1] and McCook et al. [86] supported this hypothesis finding frictional responses of PTFE to be thermally activated and consistent with van der Waals interactions. More generally, Joyce et al. [87], Brown and Dattelbaum [88], Brown et al. [89], Rae and Dattelbaum [90] and Rae and Brown [91] found similar dependencies of various mechanical properties to temperature in the range from 200 to 400 K. The measured property in each of these studies has been normalized by the room temperature measurement and is plotted versus temperature in Fig. 17.19.

Tanaka et al. [6, 18] focused on the characteristic bands of PTFE that contain both crystalline and amorphous material. In a study investigating the wear mechanisms of PTFE, they found insensitivity of wear rate to crystallinity, but found that with certain processing conditions, the characteristic size of the banded structure could be reduced with a subsequent reduction in the wear rate [6]. In varying the background temperature and sliding speed of PTFE during testing, a transition to low wear rate was found to occur as temperature increased past a critical temperature. At the 50 mm/s sliding speed used here, the data from Tanaka et al. [6] indicates a transition temperature near the IV to I phase transition of PTFE (30 °C). A recent study of the effects of PTFE phase on toughness by Brown and Dattelbaum [88] helps to explain this result. Increased fracture toughness was found for phase I ($T > 30$ °C) over phases II ($T < 19$ °C) and IV ($19 < T < 30$ °C), especially at high strain rates. Phase II was characterized by brittle fracture, while ductility and fibrillation were observed in the high toughness phase I. The fibrils were thought to bridge cracks and reduce the stress concentrations at crack tips. These results have important implications to tribology because both fracture and wear require energy to create new surfaces. These results also suggested superiority of phase I over phases II and IV in wear applications, since the events that occur in tribological contacts typically occur with high strain rates.

One constant observation in low and ultra-low wear PTFE-based composites is of fibrillation under stress at room temperature [38, 61]. SEM imaging was used to study the wear surface of a 5% 80 nm α phase alumina-PTFE nanocomposite with a wear rate of $k \sim 10^{-7}$ mm^3/N m. Figure 17.20 shows the results of these observations at two magnifications. In the low magnification image, "mudflat" cracking is observed on the wear surface. The mudflats are on the order of 10 μm in diameter and while they appear to be poorly connected to the bulk, vacancies from debris liberation are not observed. Higher

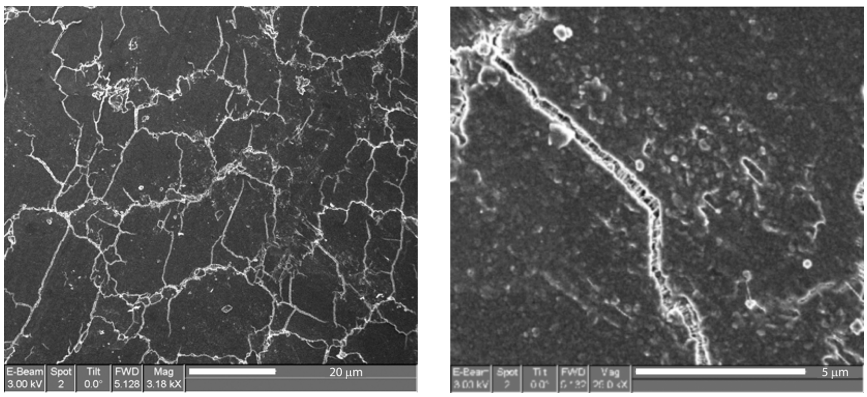

Fig. 17.20. SEM images at different magnifications of the worn surface of a 5% 80 nm α phase alumina-PTFE nanocomposite. The "mudflat" cracking is a characteristic that is repeatedly observed for these wear-resistant PTFE nanocomposites. Wear debris appears to be on the order of 1 µm, while the cracking patterns encompass 10 s of micrometers of material. The liberation of large wear debris appears to be inhibited by fibrils spanning the cracks.

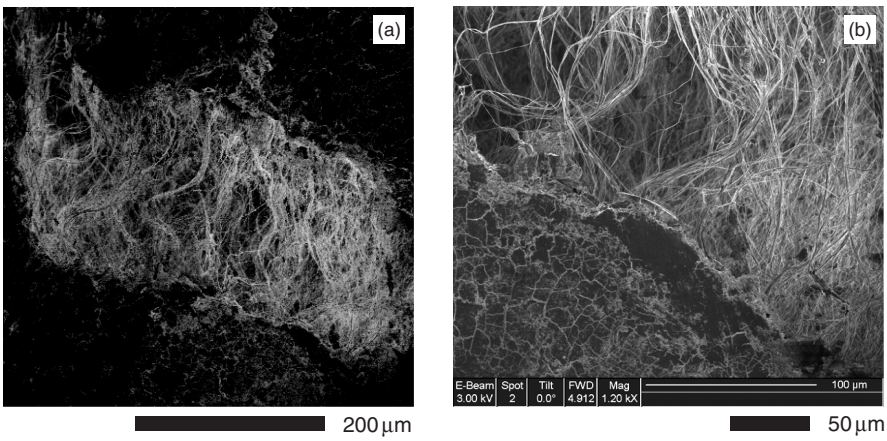

Fig. 17.21. SEM images at different magnifications of the worn surface of a 5% 80 nm α phase alumina-PTFE nanocomposite after being fractured at room temperature. Fibrils completely span a 150 µm crack.

magnification imaging reveals fibrils spanning the cracks and appearing to prevent the liberation of the cracked material as debris. The same alumina-PTFE nanocomposite was fractured in bending at 25 °C and the resulting crack imaged. This crack is shown in Fig. 17.21. Fibrils are observed to span the entire length of the 150 µm crack. This degree of fibrillation is extraordinary for PTFE under these conditions and suggests that the nanoparticles influence the crystalline morphology of the PTFE, and possibly stabilize the tougher phase I.

It is clear from the literature that the phase and morphology of PTFE are important in determining toughness and ease of fibrillation [88, 89]. It is also well known that nanoparticles can stabilize metastable crystalline phases in polymers and change the crystalline morphology [72]. Therefore, one of the mechanisms that could explain the dramatic changes in wear rate at such small filler fractions of nanoparticles is an effect of the particles on the polymer phase and morphology. The following studies were conducted to characterize the effects of the nanoparticles on the matrix to gain insights into how these morphological changes affect the tribology of PTFE.

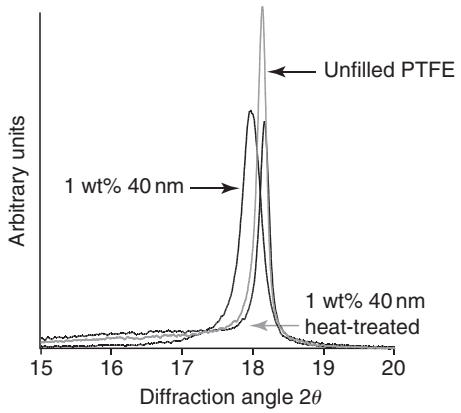

Fig. 17.22. X-Ray diffraction for the main reflections of neat PTFE, a low wear nanocomposite and the same nanocomposite after a heat treatment to 400 °C.

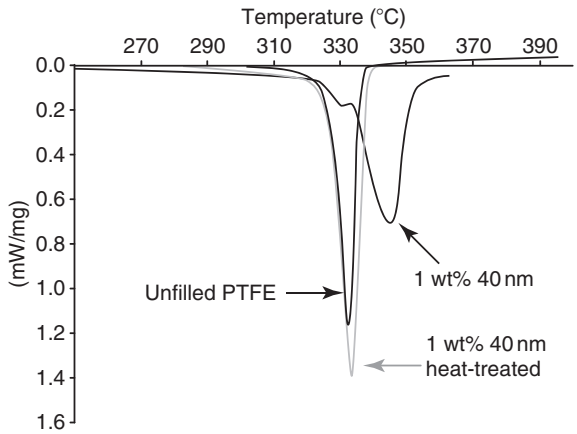

AQ9

Fig. 17.23. High temperature differential scanning calorimetry of neat PTFE, a low wear nanocomposite and the same nanocomposite after a heat treatment.

Melting behaviors of neat and filled samples were monitored using differential scanning calorimetry (DSC) and structures were examined using X-Ray diffraction (XRD) to determine the role of matrix morphology on tribological properties. The XRD patterns near the main diffraction peak (18 °) in Fig. 17.22 reveal that the nanocomposite has a larger full width half maximum (FWHM) and a larger amorphous background than the unfilled PTFE. This implies that the nanoparticles have interrupted the lamellar crystalline structure. There is also a slight shift in the peak value suggesting an interruption of the unit cell. The high-temperature DSC shown in Fig. 17.23 supports this result. The DSC shows that the degree of crystallinity of the neat matrix is significantly higher than that of the 1 wt% nanocomposite. DSC also shows a melt peak for each material near the traditional 327 °C melt temperature of PTFE. However, the nanocomposite has a larger melt peak at a higher temperature of approximately 345 °C consistent with the melt temperature of virgin PTFE before melt processing. The higher temperature is often attributed to the larger, more perfect crystals of the virgin resin. Despite being processed under identical conditions (360 °C, 4 MPa), the unfilled PTFE has melt characteristics indicative of melt-processed PTFE, while the nanocomposite retains the melt characteristics of virgin resin. The

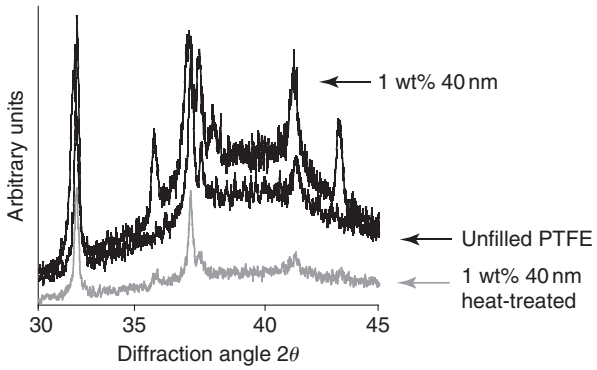

Fig. 17.24. X-Ray diffraction of neat PTFE, a low wear nanocomposite and the same nanocomposite after a heat treatment in the region sensitive to the phases present.

nanoparticles may impede the mobility of PTFE molecules, requiring greater amounts of thermal energy before reorganization of the PTFE to the lower order "gel" state can occur.

One hypothesis for wear resistance of these systems is that the virgin structure facilitates fibrillation of the nanocomposites during wear. Another is that the mechanical destruction that occurs during processing results in a fibrillated structure that is stabilized by the nanoparticles to temperatures above the process temperature; the processing involves jet-mill grinding and mixing of the powder constituents which has been shown to result in elongation and 5X size reductions of the PTFE particles [35]. In either case, higher temperatures are needed to remove any stabilized structures. To test this hypothesis, the nanofilled sample was heat-treated at 400 °C and characterized. Following heat treatment, the XRD peak at 18 ° has sharpened and returned to the same position as the unfilled PTFE.

Figure 17.24 shows that in the region most sensitive to the phases present, the 1 wt% nanofilled resin has the lowest peak height to amorphous background ratio (1.5 to 1) compared to the neat resin (3 to 1) and the heat-treated 1 wt% nanofilled resin (about 2 to 1). From the literature we know that as the proportion of phase I increases, the peaks (especially the peak at 42 °) decrease in intensity compared to the background. Because these samples are mixtures of at least two phases, it is difficult to ascertain exactly what structure is present. These results, however, imply that the 1 wt% nanofilled resin has the most phase I and the least phase IV of the materials shown and that the heat treatment to 400 °C leads to the most phase IV.

This is also supported by the DSC data at low temperature shown in Fig. 17.25. The data show that the 1 wt% nanofilled sample has much less of a phase I to IV transition than the unfilled PTFE, while the heat-treated composite shows a significant I–IV transition. Therefore, we would expect more phase I in the 1 wt% nanofilled composite and the least in the heat-treated 1 wt% nanofilled composite. In addition, the transformation temperature from I to IV is lower for the 1 wt% nanofilled sample further supporting the argument that it has the most phase I present. Finally, at room temperature the IV–II transition has begun in the heat-treated sample. This would explain the significantly higher ordering in this sample seen during XRD measurement. Both XRD and DSC provide evidence that more of the tough phase I is present in the untreated nanocomposite than either the heat-treated nanocomposite or the unfilled PTFE at room temperature. Therefore, we conclude from these results that the addition of untreated α phase nanoparticles results in a stabilization of phase I and of the local deformation that occurs during jet milling. Heat treatment at 400 °C removes these benefits and should therefore result in increased wear.

AFM was used to probe the PTFE morphologies in the nanocomposite before and after heat treatment.

The AFM measurements shown in Fig. 17.26 support the features observed in XRD and DSC. Clear differences can be seen before and after heat treatment with the nanocomposite before heat

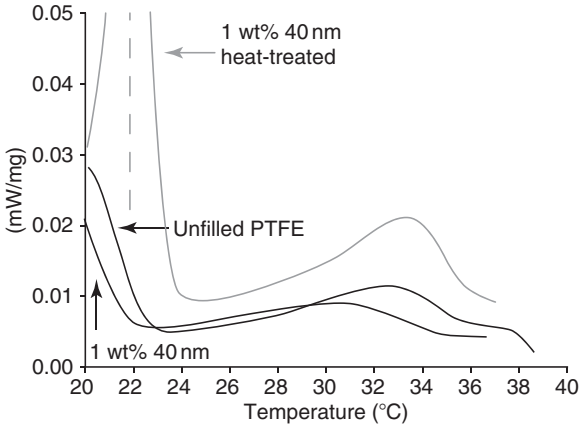

Fig. 17.25. Low temperature differential scanning calorimetry measurements of neat PTFE, a low wear nanocomposite and the same nanocomposite after a heat treatment. Stabilization of the phases to lower temperatures no longer exists after heat treatment.

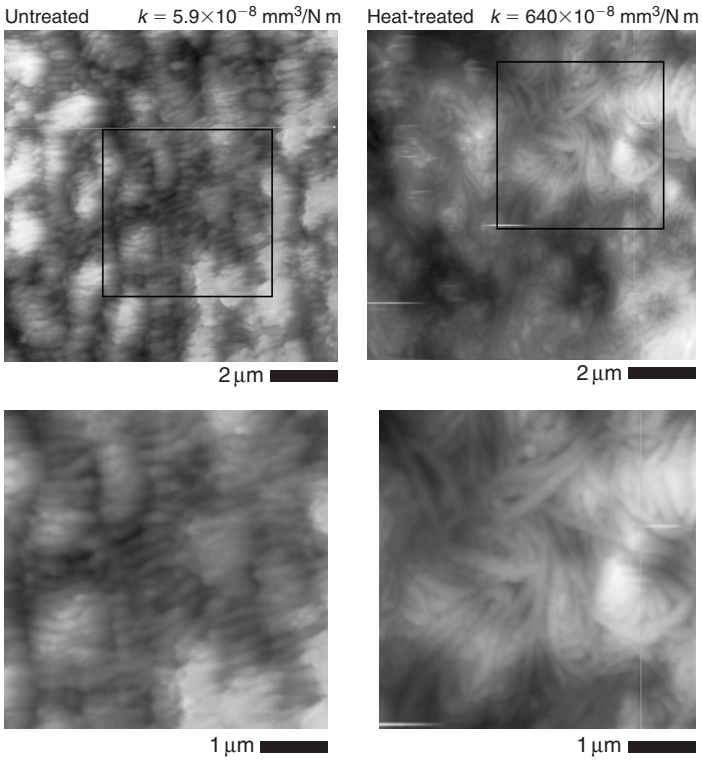

Fig. 17.26. Atomic force microscopy of the crystalline morphology of 1 wt% 40 nm alumina-PTFE before (left) and after (right) heat treatment. As-prepared, the nanocomposite has very small lamellae with finer scale, more ordered packing.

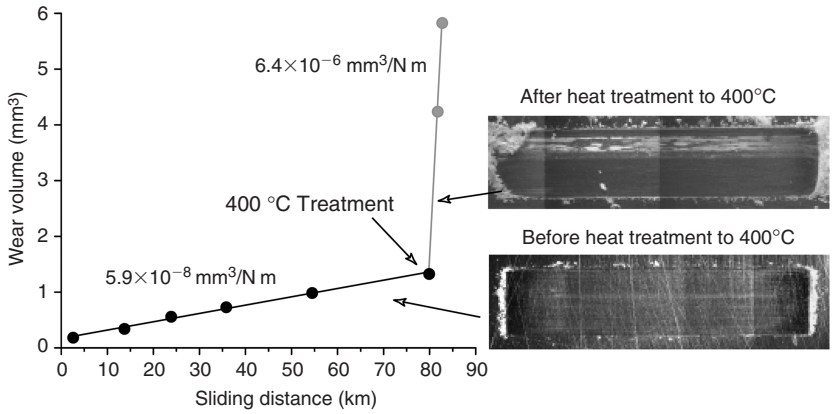

Fig. 17.27. Wear volume plotted versus sliding distance for a 1 wt% 40 nm alumina-PTFE nanocomposite before and after a heat treatment to 400 °C. The microstructural benefits of the nanoparticles are lost after heat treatment and the wear rate increases by 100X. Optical images of the transfer film before and after heat treatment are shown on the right.

treatment having much thinner and more organized lamellae than it had after heat treatment. Before heat treatment, the lamellae are well aligned and appear to have the folded-ribbon morphology that is often cited for virgin PTFE [83, 92, 93], while after heat treatment lamellae are thick, tangled and packed into substantially larger characteristic regions. Marega et al. suggest that shifts in the phase transition temperature to lower temperatures (DSC) are indicative of increased molecular disorder and thinning of lamellae [83]. XRD and AFM measurements of the control nanocomposite show evidence of increased molecular disorder and thinner lamellae, respectively. These characteristics may explain the stability of phase I for this sample at lower temperatures, and the high degree of lamellar alignment over the field of view supports the hypothesis that the nanoparticles stabilize higher melt temperatures by impeding molecular mobility.

To test the hypothesis that the effects of the nanoparticles on the morphology of PTFE reduce wear, tribological experiments were conducted on the same nanocomposite before and after heat treatment. The control experiment was conducted on the 1 wt% 40 nm α alumina-filled PTFE sample in linear reciprocation with 50% relative humidity at a temperature of 25 °C. The sliding speed and normal pressure were 50.8 mm/s and 6.3 MPa, respectively. After standard processing, the nanocomposite was tested for approximately 80 km. The sample was then heated to 400 °C to anneal the crystalline structure induced during the original processing. A new counterface was used, the sample was faced, removing only the material necessary to make it flat, and the experiment was continued. After the heat treatment, the friction coefficient was reduced by approximately 10%, wear rate increased by 100X and transfer film thickness and discontinuity increased. The tribological results are shown in Fig. 17.27. The nanoparticle phase, chemistry, size, filler fraction and dispersion are essentially constant before and after the heat treatment, so the increase in wear rate is attributed only to the morphological effects of the nanoparticles on the PTFE.

DSC and XRD measurements of a 5 wt% alumina-PTFE microcomposite were made to determine if similar morphological effects could be detected. It can be seen in Fig. 17.28 that the micrometer-scale fillers do not cause a broadening of the XRD peak at 18 ° or a shift in the peak position. This is not surprising because the scale of the particle is much larger than the lamellae size. However, the DSC and the XRD do show a lower crystallinity in the micrometer-filled sample. In addition, the XRD peaks between 30 ° and 60 ° in Fig 17.29 indicate that the micrometer-filled sample has a large amorphous peak, but the peak to amorphous background ratio is 2 to 1 compared to that in the 1 wt% nanofilled sample indicating a higher percentage of phase I in the nanofilled sample.

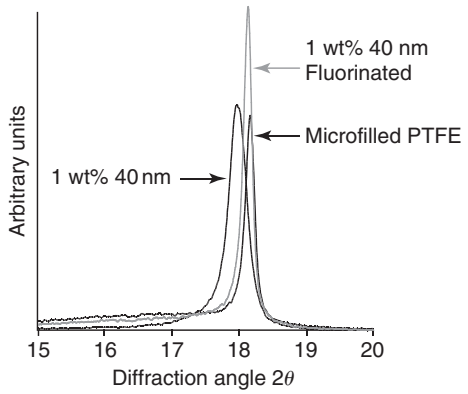

Fig. 17.28. X-Ray diffraction of a microcomposite and fluorinated and virgin alumina nanocomposites in the region of the primary reflection.

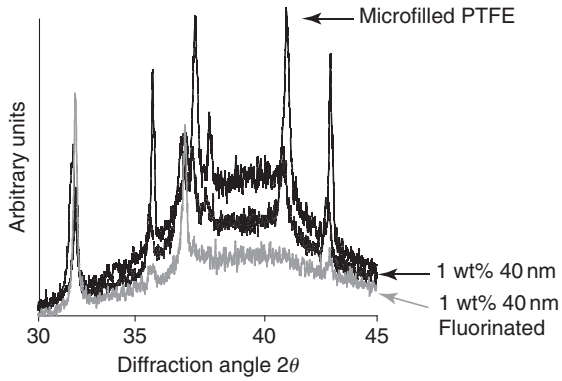

Fig. 17.29. X-Ray diffraction of a microcomposite and fluorinated and virgin alumina nanocomposites in the region sensitive to the phases present.

Similar experiments were conducted on fluorinated alumina-PTFE nanocomposites to investigate the roles of phase and morphology on the wear rates of these systems. Unlike the control nanocomposite, the fluorinated nanocomposite had a melt temperature near 327 °C, the low temperature peak. The XRD peak at 18 ° shown in Fig. 17.28 has a FWHM similar to that of the unfilled PTFE with no peak shift. This implies that the nanoparticles have not interrupted the lamellar structure, or the unit cell. In addition, for the 30 °–60 ° region, the peak at 42 ° is absent in this sample. This indicates that the sample is primarily phase I. The room temperature DSC data shown in Fig. 17.30 is less clear. The phase I–IV transformation is small in the fluorinated material, but no smaller than in the as received 1 wt% nanocomposite. While the temperature shift is less extreme for the fluorinated sample compared to the control sample, there is a longer tail of material transitioning at temperatures well below the transition temperature.

AQ3

The fluorinated sample had comparable wear resistance to the control nanocomposite sample, but it lacked some of the distinct morphological differences, such as interruption of the lamellar structure and unit cell, and high melt temperature, that were hypothesized to be responsible for wear resistance. It did however show a strong phase I character in XRD and a shift in phase transitions to lower temperatures in DSC. It was therefore hypothesized that one of the critical roles of the nanoparticles was the stabilization

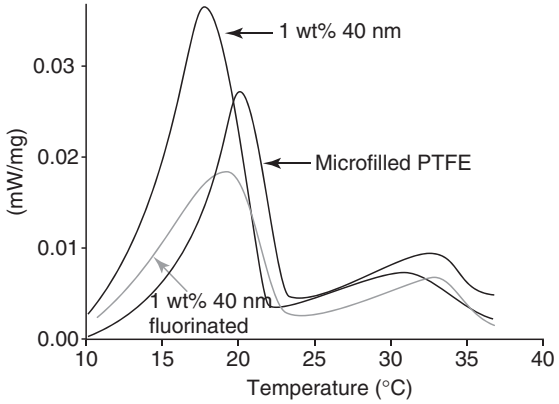

Fig. 17.30. Low temperature differential scanning calorimetry measurements of a microcomposite and fluorinated and untreated alumina nanocomposites.

of the high toughness phase I at the test temperature. The previous DSC data indicate that the phase II transition of the control nanocomposite occurs at a temperature of 18 °C. Thus if stabilization of phase I or IV leads to low wear at room temperature, then the wear rate of this sample should increase as temperature is reduced below some critical temperature near 18 °C. To isolate the effects of thermal history from phase stabilization, an additional nanocomposite test specimen was cut from the original low wear 1 wt% 40 nm α phase alumina-PTFE puck described earlier. The sample was run-in on a fresh counterface for 2,500 m of sliding with 6.3 MPa of pressure at 40 °C. The wear rate during run-in was 6×10^{-7} mm^3/N m, consistent with the run-in observed in the original experiment. Forecasting from the initial experiment, the wear rate after a 2,500 m run-in is near steady state and on the order of $k \sim 10^{-7}$ mm^3/N m. After an additional 25 m of sliding, the temperature was continuously decreased over the next 30 m to a target of 10 °C; the dew point temperature was approximately 7–8 °C.

The results of the varied temperature experiment are shown in Fig. 17.31 with wear rate and counterface temperature plotted as functions of sliding distance. The wear rate curve was estimated from mass loss measurements and in situ observation of the transition. The data shown here were recorded after the initial run-in period. For the first 47 m of sliding, no observable debris was liberated from the contact indicating retention of the low wear state. At 47 m, the temperature was 14 °C and the first wear fragment appeared. This was followed by rapid deterioration of performance until a steady state wear rate of $k \sim 5 \times 10^{-4}$ mm^3/N m was reached at 52 m and approximately 12 °C.

It was hypothesized that the wear resistance of the nanocomposite was due to a disruption of the crystalline structure by the nanoparticles that resulted in increased disorder, stabilization of the higher toughness phase to lower temperatures and fibrillation under stress. The results from DSC of this sample are plotted versus temperature in Fig. 17.32.

The transition to high wear occurs when most of the sample has transitioned to the low toughness phase II. In addition to being more brittle, Brown et al. [89] found phase II to be stronger and stiffer than phases I and IV. It is possible that as temperature is dropped and the material begins to transit to phase II, deformation preferentially occurs in the remaining phase IV material. At a critical point, enough of the material has been converted such that phase II must contribute to motion accommodation. Eventually, crack initiation, propagation and gross failure occur. The fact that unfilled PTFE does not exhibit such high wear resistance at comparable locations on the phase diagram suggests that facilitation of fibril formation is an additional critical wear resistance mechanisms in PTFE nanocomposites. The breakdown of wear performance coinciding with transition to phase II suggests that the beneficial fibril-related toughening mechanism that results from the nanoparticle filler, is disabled in phase II.

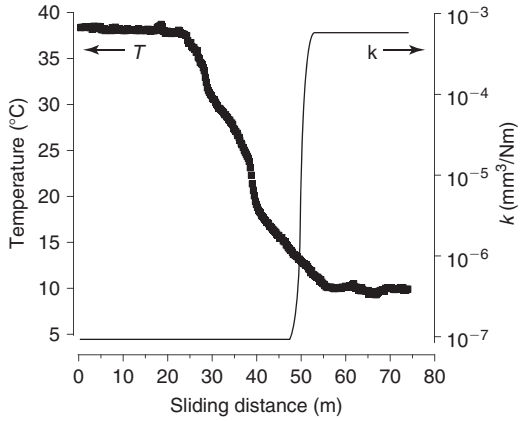

Fig. 17.31. Wear rate and counterface temperature versus sliding distance for variable temperature tribology testing of a wear-resistant PTFE nanocomposite. Wear rate is an estimate based on mass measurements and in-situ observation of the transition. Normal pressure and sliding speed were 6.3 MPa and 50 mm/s, respectively. An abrupt and drastic change in the wear mechanism occurs as the temperature is reduced below about 14 °C.

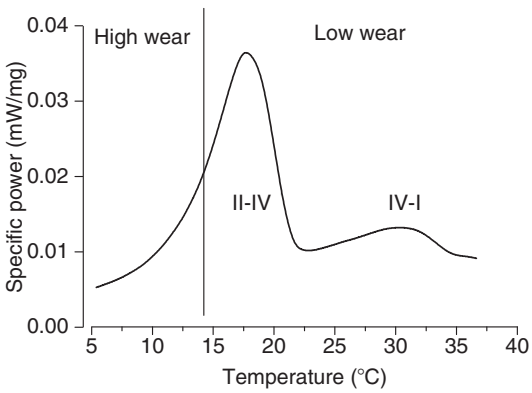

Fig. 17.32. Normalized DSC power plotted versus temperature. The transition to high wear occurs at a critical point after the low toughness phase II transition temperature.

17.3 Hypothesized Model of Wear Resistance Mechanisms in PTFE Solid Lubricants

17.3.1 Introduction

Though many future studies are still needed to complete our understanding of these systems, the material science characterization and tribology literatures combined with the recent studies just discussed have helped shape a more complete understanding of PTFE nanocomposites' tribology. The previously discussed research has shown that many factors have direct effects on the tribology of PTFE and suggests the degree of complexity that arises as these factors couple together to determine global tribosystem characteristics. We will now discuss a hypothesis for wear and wear resistance mechanisms of PTFE-based systems.

17.3.2 Wear of unfilled PTFE

In unfilled PTFE, low toughness and easy slip of internal interfaces dominates the wear rate. Below the critical speed, the friction coefficient at the tribological interface is low and statically loaded internal interfaces of self-mated PTFE can fully support the traction. In this situation, adhesive and abrasive wear dominate and lead to wear rates on the order of $k \sim 10^{-5}$ mm^3/N m. Above the critical speed, the friction coefficient at the tribological interface exceeds that at internal interfaces, cracks rapidly propagate and severe wear occurs ($k \sim 10^{-3}$ mm^3/N m) [1]. The thick, plate-like debris deposited onto the counterface are easily ejected from the contact by the passing pin.

17.3.3 Wear of PTFE microcomposites

Microscale fillers have been successfully used to arrest the crack propagation that leads to severe delamination wear in PTFE. As a crack encounters a particle, it is deflected or arrested and debris size is reduced. Because cracks can travel readily through unreinforced PTFE, the interparticle spacing is a critical parameter. Often, high filler fractions of these particles are required to limit this spacing, to provide load support against asperity contact and ultimately, to improve wear performance. These fillers must themselves be hard and wear-resistant to promote wear resistance of the system and often abrade transfer films and counterfaces. We have shown that as particle size is reduced from the micrometer-scale to the nanoscale, a transition from moderate wear ($k \sim 10^{-5}$ mm^3/N m) to low wear ($k \sim 10^{-7}$ mm^3/N m) can occur. It was also shown that the introduction of micrometer fillers to a low wear nanocomposite disrupts the wear resistance mechanisms of the nanocomposite and the system transitions to moderate wear. Observations of gross destruction of the composite and abraded counterfaces and transfer films suggest that micrometer fillers prevent low wear by abrading the transfer films needed for protection against direct asperity contact.

17.3.4 Wear of PTFE nanocomposites

To facilitate discussions of the various coupled interactions that occur in PTFE nanocomposites, we will describe wear resistance mechanisms as being either primary or secondary. A wear resistance mechanism is defined here as a property or effect that has been shown to have a direct impact upon the wear rate. A primary wear resistance mechanism is defined here as one that requires no pre-existing condition of wear resistance to occur, while a secondary wear resistance mechanism occurs only as a result of wear resistance. Primary wear resistance mechanisms that have been identified include: (1) bonding and strength at the filler/matrix interface, (2) dispersion and mechanical effects of load support and crack deflection, (3) morphological effects of nanoparticles on the matrix and (4) fibrillation and toughening. Secondary wear resistance mechanisms that have been identified include: (1) transfer film protection, (2) transfer film orientation and (3) chemical degradation. The hypothetical system shown in Fig. 17.33 illustrates each of these mechanisms, highlighting the interactions of these different primary and secondary wear resistance mechanisms.

Bonding at the filler/matrix interface occurs over the smallest length scales, involving both entanglement of individual chains and chemical bonds between atoms. Because particle densities and specific areas are inherently large in nanocomposites, subtle differences in the bonding state between a matrix chain and filler particle can translate into substantial improvements to bulk properties. Such differences are thought to be responsible for the superior wear resistance of α phase alumina-filled PTFE over Δ:Γ phase alumina-filled PTFE. There is also evidence to suggest that activation and effectiveness of the other mechanisms depends on the nature of the filler/matrix interface.

At a larger size scale, nanoparticle dispersion provides an additional mechanism of wear resistance by interfering with crack propagation and by shielding the matrix from direct asperity contact. Because low

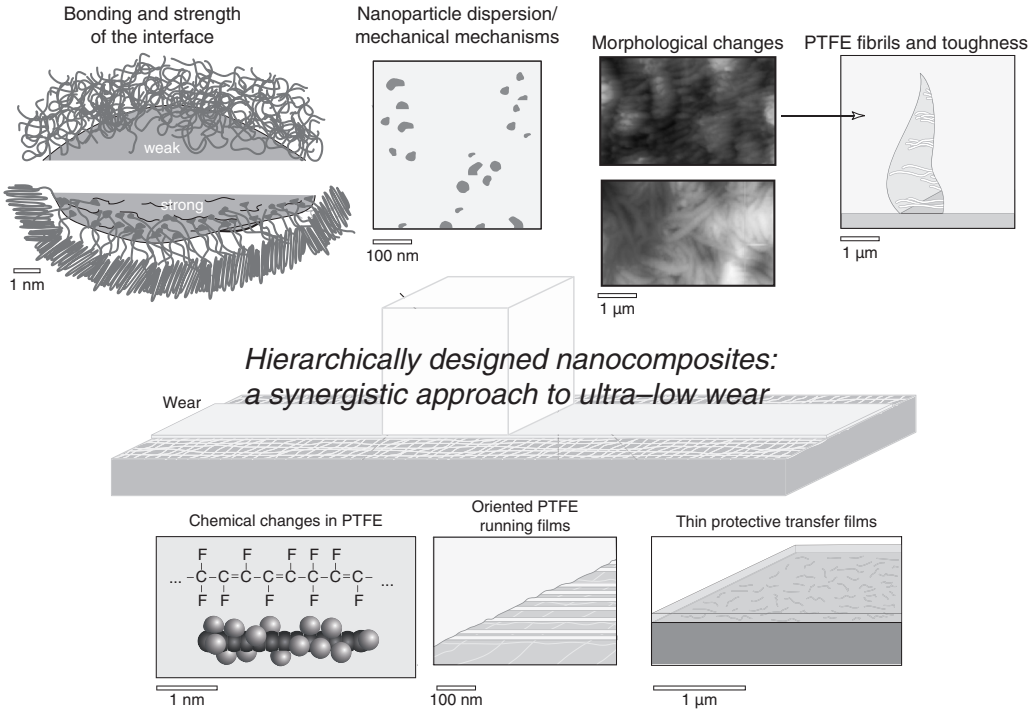

Fig. 17.33. Hypothetical model of a PTFE-based tribological nanocomposite. Arrows point from cause to effect. Thin, aligned and degraded transfer films are thought to develop as a result of low wear debris morphology and once initiated, provide low wear feedback into the system.

filler fractions are desirable, the direct mechanical effects of the nanoparticles are thought to be minimal, e.g. Δ:Γ nanocomposites. Both interfacial strength and nanoparticle dispersion determine the effectiveness of crack arrestment. When the filler/matrix interface is weak, particles arrest cracks less effectively and may actually nucleate additional cracks. When nanoparticle dispersion is poor, interparticle distance is large, and cracks may freely propagate through unfilled material. Additionally, nanocomposites with agglomerations may be brittle because agglomerations are poorly bound by matrix material.

If the nanoparticles are well dispersed, strong interactions at the nanoparticle surface can influence the crystalline phase and morphology on a micrometer size scale. Smaller lamellar thickness and increased molecular disorder can stabilize a higher toughness phase. In addition, these morphological effects are thought to determine the composite's ability to fibrillate. When fibrillation is activated, extensive deformation is required before material removal can occur.

When the debris size is sufficiently reduced via primary wear resistance mechanisms, secondary mechanisms are activated. During sliding, the highly deformed and fibrillated matrix is easily drawn into thin oriented films that protect the composite from asperity damage and facilitate low shear sliding. As wear rate is reduced, material is resident at the interface longer, more frictional energy is absorbed and degradation produces more wear-resistant, conjugated PTFE.

17.3.5 Summary

Results of these studies support many of the consistent observations found in the PTFE nanocomposites tribology literature, and more generally, the polymer nanocomposite tribology literature. Additionally,

these results provide quantitative evidence to support previous qualitative observations from the literature. The contributions of the nanoparticles span well beyond the traditional rules of mixtures models that adequately describe many of the commercial PTFE microcomposites, with nanoparticle dispersion, surface morphology and chemistry likely driving the fundamental wear resistance mechanisms that synergistically couple to produce low wear. Currently, it is difficult to make a global interpretation of the state of the art of PTFE nanocomposite tribology because of the inherently large number of variables and the limited number of quantitative measurements of these different variables; critical components such as nanoparticle dispersion are almost completely absent from discussion in the literature (this work included). We have gathered results and offered a hypothesis based on a limited but ongoing research initiative to promote thought and discussion, provide new insights into overlooked aspects of the literature and motivate future, directed studies of these systems. The authors believe that with independent and quantitative materials and tribological characterization, great strides will soon be made in constructing a more accurate and complete description of these systems to enable novel composite design for current and future needs.

Acknowledgments

This material is based upon an AFOSR-MURI grant FA9550-04-1-0367. Any opinions, findings and conclusions or recommendations expressed in this material are those of the authors and do not necessarily reflect the views of the Air Force Office of Scientific Research. We would like to thank Will Heward for the X-Ray diffraction work, Su Zhao for particle surface fluorination and Sashi Kandanur and Steven McElwain for tribological experimentation.

References

[1] T. Blanchet, F. Kennedy, Sliding wear mechanism of polytetrafluoroethylene (PTFE) and PTFE composites. Wear, 153(1) (1992) 229–243.
[2] D. Flom, N. Porile, Friction of teflon sliding on teflon. J. Appl. Phys., 26(9) (1955) 1088–1092.
[3] K. Makinson, D. Tabor, Friction + transfer of polytetrafluoroethylene. Nature, 201(491) (1964) 464.
[4] K. Mclaren, D. Tabor, Visco-elastic properties and friction of solids – friction of polymers – influence of speed and temperature. Nature, 197(487) (1963) 856.
[5] R. Steijn, Sliding experiments with polytetrafluoroethylene. Asle Transact., 11(3) (1968) 235.
[6] K. Tanaka, Y. Uchiyama, S. Toyooka, Mechanism of wear of polytetrafluoroethylene. Wear, 23(2) (1973) 153–172.
[7] C. Bunn, A. Cobbold, R. Palmer, The fine structure of polytetrafluoroethylene. J. Poly. Sci., 28(117) (1958) 365–376.
[8] C. Speerschneider, C. Li, Some observations on structure of polytetrafluoroethylene. J. Appl. Phys., 33(5) (1962) 1871–.
[9] N. Suh, Delamination theory of wear. Wear, 25(1) (1973) 111–124.
[10] S. Bahadur, D. Gong, The action of fillers in the modification of the tribological behavior of polymers. Wear, 158(1–2) (1992) 41–59.
[11] T. Blanchet, Y. Peng, Wear resistant irradiated FEP unirradiated PTFE composites. Wear, 214(2) (1998) 186–191.
[12] B. Burroughs, J. Kim, T. Blanchet, Boric acid self-lubrication of B2O3-filled polymer composites. Tribol. Trans., 42(3) (1999) 592–600.
[13] F. Li et al., The tribological behaviors of copper-coated graphite filled PTFE composites. Wear, 237(1) (2000) 33–38.
[14] Z. Lu, K. Friedrich, On sliding friction and wear of PEEK and its composites. Wear, 181 (1995) 624–631.
[15] B. Menzel, T. Blanchet, Effect of particle size and volume fraction of irradiated FEP filler on the transfer wear of PTFE. Lubr. Eng., 58(9) (2002) 29–35.

AQ4

[16] J. K. Lancaster, Polymer-based bearing materials – role of fillers and fiber reinforcement in wear. Wear, 22(3) (1972) 412–.
[17] N. Sung, N. Suh, Effect of fiber orientation on friction and wear of fiber reinforced polymeric composites. Wear, 53(1) (1979) 129–141.
[18] K. Tanaka, S. Kawakami, Effect of various fillers on the friction and wear of polytetrafluoroethylene-based composites. Wear, 79(2) (1982) 221–234.
[19] B. Briscoe, A. Pogosian, D. Tabor, Friction and wear of high-density polythene – action of lead oxide and copper oxide fillers. Wear, 27(1) (1974) 19–34.
[20] D. Gong, Q. Xue, H. Wang, ESCA study on tribochemical characteristics of filled PTFE. Wear, 148(1) (1991) 161–169.
[21] D. Gong et al., Effect of tribochemical reaction of polytetrafluoroethylene transferred film with substrates on Its wear behavior. Wear, 137(2) (1990) 267–273.
[22] T. Blanchet, F. Kennedy, D. Jayne, XPS analysis of the effect of fillers on PTFE transfer film development in sliding contacts. Tribol. Transact., 36(4) (1993) 535–544.
[23] S. Bahadur, D. Tabor, The wear of filled polytetrafluoroethylene. Wear, 98(1–3) (1984) 1–13.
[24] B. Ash, L. Schadler, R. Siegel, Glass transition behavior of alumina/polymethylmethacrylate nanocomposites. Mater. Lett., 55(1–2) (2002) 83–87.
[25] A. Eitan et al., Reinforcement mechanisms in MWCNT-filled polycarbonate. Compos. Sci. Technol., 66(9) (2006) 1162–1173.
[26] C. Ng, L. Schadler, R. Siegel, Synthesis and mechanical properties of TiO_2-epoxy nanocomposites. Nanostruct. Mater., 12(1–4) (1999) 507–510.
[27] A. Zhu, S. Sternstein, Nonlinear viscoelasticity of nanofilled polymers: interfaces, chain statistics and properties recovery kinetics. Compos. Sci. Technol., 63(8) (2003) 1113–1126.
[28] O. Wang, Q. Xue, W. Shen, The friction and wear properties of nanometre SiO_2 filled polyetheretherketone. Tribol. Int., 30(3) (1997) 193–197.
[29] Q. Wang et al., An investigation of the friction and wear properties of nanometer Si3N4 filled PEEK. Wear, 196(1–2) (1996) 82–86.
[30] Q. Wang et al., The effect of particle size of nanometer ZrO_2 on the tribological behaviour of PEEK. Wear, 198(1–2) (1996) 216–219.
[31] Q. Wang et al., The friction and wear characteristics of nanometer SiC and polytetrafluoroethylene filled polyetheretherketone. Wear, 243(1–2) (2000) 140–146.
[32] Q. Xue, Q. Wang, Wear mechanisms of polyetheretherketone composites filled with various kinds of SiC. Wear, 213(1–2) (1997) 54–58.
[33] F. Li et al., The friction and wear characteristics of nanometer ZnO filled polytetrafluoroethylene. Wear, 249(10–11) (2001) 877–882.
[34] W. Chen et al., Tribological behavior of carbon-nanotube-filled PTFE composites. Tribol. Lett., 15(3) (2003) 275–278.
[35] W. Sawyer et al., A study on the friction and wear behavior of PTFE filled with alumina nanoparticles. Wear, 254(5–6) (2003) 573–580.
[36] D. Burris, W. Sawyer, Tribological sensitivity of PTFE/Alumina nanocomposites to a range of traditional surface finishes. Tribol. Trans., 48(2) (2005) 147–153.
[37] D. Burris, W. Sawyer, Improved wear resistance in alumina-PTFE nanocomposites with irregular shaped nanoparticles. Wear, 260(7–8) (2006) 915–918.
[38] S. Mcelwain, Wear resistant PTFE composites via nano-scale particles. Master's Thesis, Rensselaer Polytechnic Institute, Troy, New York, 2006.
AQ5 [39] S. Kandanur, Master of science thesis. Rensselaer Polytechnic Institute, Tory, New York, 2007.
[40] S. Han, T. Blanchet, Experimental evaluation of a steady-state model for the wear of particle-filled polymer composite materials. J. Tribol. Trans. ASME, 119(4) (1997) 694–699.
[41] P. Bhimaraj et al., Effect of matrix morphology on the wear and friction behavior of alumina nanoparticle/poly(ethylene) terephthalate composites. Wear, 258(9) (2005), 1437–1443.
[42] C. Schwartz, S. Bahadur, Studies on the tribological behavior and transfer film-counterface bond strength for polyphenylene sulfide filled with nanoscale alumina particles. Wear, 237(2) (2000) 261–273.

[43] G. Beamson et al., Characterization of PTFE on silicon wafer tribological transfer films by XPS, imaging XPS and AFM. Surf. Interface Anal., 24(3) (1996) 204–.
[44] D. Breiby et al., Structural surprises in friction-deposited films of poly(tetrafluoroethylene). Macromolecules, 38(6) (2005) 2383–2390.
[45] C. Pooley, D. Tabor, Friction and molecular structure – behavior of some thermoplastics. Proc. R. Soc. Lond. Ser. A: Math. Phys. Sci., 329(1578) (1972) 251–.
[46] D. Wheeler, The transfer of polytetrafluoroethylene studied by X-Ray photoelectron-spectroscopy. Wear, 66(3) (1981) 355–365.
[47] J. Wittmann, P. Smith, Highly oriented thin-films of poly(tetrafluoroethylene) as a substrate for oriented growth of materials. Nature, 352(6334) (1991) 414–417.
[48] T. Blanchet, A model for polymer composite wear behavior including preferential load support and surface accumulation of filler particulates. Tribol. Trans., 38(4) (1995) 821–828.
[49] S. Abdou, R. Mohamed, Characterization of structural modifications in poly-tetrafluoroethylene induced by electron beam irradiation. J. Phys. Chem. Solid., 63(3) (2002) 393–398.
[50] B. Briscoe, H. Mahgerefteh, S. Suga, The effect of gamma irradiation on the pressure dependence of the room temperature transition in PTFE. Polymer, 44(3) (2003) 783–791.
[51] B. Fayolle, L. Audouin, J. Verdu, Radiation induced embrittlement of PTFE. Polymer, 44(9) (2003) 2773–2780.
[52] O. Harling, G. Kohse, K. Riley, Irradiation performance of polytetrafluoroethylene (teflon(R)) in a mixed fast neutron and gamma radiation field. J. Nucl. Mater., 304(1) (2002) 83–85.
[53] X. Zhao et al., An experimental study of low earth orbit atomic oxygen and ultraviolet radiation effects on a spacecraft material – polytetrafluoroethylene. Polym. Degrad. Stabil., 88(2) (2005) 275–285.
[54] H. Dorschner, U. Lappan, K. Lunkwitz, Electron beam facility in polymer research: Radiation induced functionalization of polytetrafluoroethylene. Nucl. Instrum. Met. Phys. Res. Sect. B – Beam Interact. Mater. Atoms, 139(1–4) (1998) 495–501.
[55] U. Lappan et al., Number-average molecular weight of radiation-degraded poly(tetrafluoroethylene). An end group analysis based on solid-state NMR and IR spectroscopy. Polymer, 43(16) (2002) 4325–4330.
[56] U. Lappan et al., Radiation-induced branching and crosslinking of poly(Tetrafluoroethylene) (PTFE). Nucl. Instrum. Met. Phys. Res. Sect. B: Beam Interact. Mater. Atoms, 185 (2001) 178–183.
[57] A. Oshima et al., Chemical structure and physical properties of radiation-induced crosslinking of polytetrafluoroethylene. Rad. Phys. Chem., 62(1) (2001) 39–45.
[58] E. Katoh et al., Evidence for radiation induced crosslinking in polytetrafluoroethylene by means of high-resolution solid-state F-19 high-speed MAS NMR. Rad. Phys. Chem., 54(2) (1999) 165–171.
[59] B. Fuchs, U. Scheler, Branching and cross-linking in radiation-modified poly(tetrafluoroethylene): A solid-state NMR investigation. Macromolecules, 33(1) (2000) 120–124.
[60] T. Blanchet, Y. Peng, Wear-resistant polytetrafluoroethylene via electron irradiation. Lubr. Eng., 52(6) (1996) 489–495.
[61] D. Burris, W. Sawyer, A low friction and ultra low wear rate PEEK/PTFE composite. Wear, 261(3–4) (2006) 410–418.
[62] D. Wagner, R. Vaia, Nanocomposites: Issues at the interface. Mater. Today, (2004) 38—42.
[63] P. He et al., Surface modification and ultrasonication effect on the mechanical properties of carbon nanofiber/polycarbonate composites. Compos. Part A – Appl. Sci. Manuf., 37(9) (2006) 1270–1275.
[64] S. Sternstein et al., Reinforcement and nonlinear viscoelasticity of polymer melts containing mixtures of nanofillers. Rubber Chem. Technol., 78(2) (2005) 258–270.
[65] M. Maiti, A. Bhowmick, New insights into rubber-clay nanocomposites by AFM imaging. Polymer, 47(17) (2006) 6156–6166.
[66] H. Koerner et al., Deformation-morphology correlations in electrically conductive carbon nanotube thermoplastic polyurethane nanocomposites. Polymer, 46(12) (2005) 4405–4420.
[67] D. Ratna et al., Poly(ethylene oxide)/clay nanocomposite: Thermomechanical properties and morphology. Polymer, 47(11) (2006) 4068–4074.
[68] K. Yang et al., Morphology and mechanical properties of polypropylene/calcium carbonate nanocomposites. Mater. Lett., 60(6) (2006) 805–809.

AQ6

[69] A. Yasmin et al., Mechanical and thermal behavior of clay/epoxy nanocomposites. Compos. Sci. Technol., 66 (2006) 2415–2422.
[70] Y. Kojima et al., Mechanical-properties of nylon 6-clay hybrid. J. Mater. Res., 8(5) (1993) 1185–1189.
[71] H. Yang et al., Crystal growth in alumina/poly(ethylene terephthalate) nanocomposite films. J. Polym. Sci. Part B: Polym. Phys., (2006 (submitted)).
[72] Z. Xiao et al., Probing the use of small-angle light scattering for characterizing structure of titanium dioxide/low-density polyethylene nanocomposites. J. Polym. Sci. Part B – Polym. Phys., 44(7) (2006) 1084–1095.
[73] E. Petrovicova et al., Nylon 11/silica nanocomposite coatings applied by the HVOF process. I. Microstructure and morphology. J. Appl. Poly. Sci., 77(8) (2000) 1684–1699.
[74] F. Kuchta et al., Materials with improved properties from polymer-ceramic-nanocomposites. Mat. Res. Soc. Symp. Proc., 576 (1999) 363–368.
[75] E. Clark, The molecular conformations of polytetrafluoroethylene: Forms II and IV. Polymer, 40(16), (1999) 4659–4665.
[76] J. Weeks, E. Clark, R. Eby, Crystal-structure of the low-temperature phase(II) of polytetrafluoroethylene. Polymer, 22(11) (1981) 1480–1486.
[77] J. Weeks, R. Eby, E. Clark, Disorder in the crystal-structures of phase-1 and phase-2 of copolymers of tetrafluoroethylene and hexafluoropropylene. Polymer, 22(11) (1981) 1496–1499.
[78] B. Farmer, R. Eby, Energy calculations of the crystal-structure of the low-temperature phase (II) of polytetrafluoroethylene. Polymer, 22(11) (1981) 1487–1495.
[79] C. Bunn, E. Howells, Structures of molecules and crystals of fluorocarbons. Nature, 174(4429) (1954) 549–551.
[80] H. Rigby, C. Bunn, A room-temperature transition in polytetrafluoroethylene. Nature, 164(4170) (1949) 583–583.
[81] M. Kimmig, G. Strobl, B. Stuhn, Chain reorientation in poly(tetrafluoroethylene) by mobile twin-helix reversal defects. Macromolecules, 27(9) (1994) 2481–2495.
[82] F. Tieyuan et al., Study of factors affecting room temperature transition of polytetrafluoroethylene. Chinese J. Polym. Sci., 2 (1986) 170–179.
[83] C. Marega et al., Relationship between the size of the latex beads and the solid-solid phase transitions in emulsion polymerized poly(tetrafluoroethylene). Macromolecules, 37(15) (2004) 5630–5637.
[84] M. D'amore et al., Disordered chain conformations of poly(tetrafluoroethylene) in the high-temperature crystalline form I. Macromolecules, 37(25) (2004) 9473–9480.
[85] H. Ting-Yung, N. Eiss, Effects of molecular weight and crystallinity on wear of polytetrafluoroethylene. Wear of Materials: International Conference on Wear of Materials, pp. 636–642 (1983).
[86] N. McCook et al., Cryogenic friction behavior of PTFE based solid lubricant composites. Tribol. Lett., 20(2) (2005) 109–113.
[87] J. Joyce, Fracture toughness evaluation of polytetrafluoroethylene. Polymer Eng. Sci., 43(10) (2003) 1702–1714.
[88] E. Brown, D. Dattelbaum, The role of crystalline phase on fracture and microstructure evolution of polytetrafluoroethylene (PTFE). Polymer, 46(9) (2005) 3056–3068.
[89] E. Brown et al., The effect of crystallinity on the fracture of polytetrafluoroethylene (PTFE). Mater. Sci. Eng. C-biomimetic Supramole. Syst., 26(8) (2006) 1338–1343.
[90] P. Rae, D. Dattelbaum, The properties of poly(tetrafluoroethylene) (PTFE) in compression. Polymer, 45(22) (2004) 7615–7625.
[91] P. Rae, E. Brown, The properties of poly(tetrafluoroethylene) (PTFE) in tension. Polymer, 46(19) (2005) 8128–8140.
[92] R. Pucciariello, V. Villani, Phase behavior at low temperature of poly(tetrafluoroethylene) by temperature-modulated calorimetry. J. Fluorine Chem., 125(2) (2004) 293–302.
[93] R. Pucciariello, V. Villani, Melting and crystallization behavior of poly (tetrafluoroethylene) by temperature modulated calorimetry. Polymer, 45(6) (2004) 2031–2039.

Author Queries

AQ1: 'Trimethyoxysilane' has been changed to 'trimethoxysilane' in the sentence "The 40 nm α phase …". Is this OK?
AQ2: Can 1/8% be changed to 0.125% in the sentence "The wear rates of the functional…". Please confirm.
AQ3: Please check the sense of the sentence "The phase I–IV transformation…"
AQ4:Please check the page range in refs [8], [16], [43], and [45].
AQ5: Please provide article title in ref. [39].
AQ6: Please provide volume number in ref. [62].
AQ7: Please provide volume number and page range in ref. [71].
AQ8: Please provide all the author names in the refs [13], [21], [25], [29], [33–35], [41], [43], [44], [53], [55], [57], [58], [63], [64], [66], [68–74], [82–84], [86] and [89].
AQ9: Please define the variable plotted in the X-axis in the Figs. 17.23, 17.25, and 17.30.